Replacing carbon cloth by nickel mesh as substrate for air-diffusion cathodes: H_2O_2 production and carbenicillin degradation by photoelectro-Fenton

Gengbo Ren[a,b,c], Sonia Lanzalaco[d], Minghua Zhou[b,**], Pere L. Cabot[a], Enric Brillas[a], Ignasi Sirés[a,*]

[a] *Laboratori d'Electroquímica dels Materials i del Medi Ambient, Departament de Ciència de Materials i Química Física, Secció de Química Física, Facultat de Química, Universitat de Barcelona, Martí i Franquès 1-11, 08028 Barcelona, Spain*

[b] *Key Laboratory of Pollution Process and Environmental Criteria, Ministry of Education, College of Environmental Science and Engineering, Nankai University, 300350 Tianjin, China*

[c] *School of Energy and Environment Engineering, Hebei University of Technology, Tianjin 300401, China*

[d] *Departament d'Enginyeria Química and Barcelona Research Center in Multiscale Science and Engineering, EEBE, Universitat Politècnica de Catalunya, C/Eduard Maristany, 10-14, 08019 Barcelona, Spain*

Paper submitted to be published in *Chemical Engineering Journal*

* Corresponding author: *E-mail address*: i.sires@ub.edu (I. Sirés)

** Corresponding author: *E-mail address*: zhoumh@nankai.edu.cn (M. Zhou)

Abstract

The development of air-diffusion electrodes (ADEs) that electrocatalytically produce H_2O_2 for its decomposition by Fenton's reaction is gaining relevance. However, attention has been paid to improve the catalytic layer using standard carbonaceous substrates like C_{cloth}. This work clearly proves the superior endurance of 3 cm^2 ADEs fabricated with Ni_{mesh} as substrate, achieving stable H_2O_2 accumulation up to 60 mM at 100 mA for 48 h in an undivided cell. Consequently, the antibiotic carbenicillin could be totally degraded in 13 min by photoelectro-Fenton (PEF) process using the Ni_{mesh}|C-PTFE ADE at 20 mA in an acidic model solution. This high performance was confirmed by PEF treatment in urban wastewater, reaching total drug disappearance in 18 min with more than 80% TOC abatement. The time course of $^{\bullet}OH$ and toxicity was monitored, whereas chromatographic analysis of treated solutions revealed the formation of 32 aromatic and 16 aliphatic byproducts, including 7 linear carboxylic acids.

Keywords: Air-diffusion electrode (ADE); Antibiotic; Hydrogen peroxide electrosynthesis; Ni mesh; Water treatment

1. Introduction

In the last 20 years, threats to the aqueous environment have ceaselessly diversified and multiplied [1,2] and, nowadays, it is assumed that global strategies are required to face menaces that overstep local boundaries [3]. Lately, the occurrence of antibiotics in water bodies has been identified as particularly troublesome [4], since despite being classified as trace organic chemicals (TOrCs) [5], they promote bacterial resistance that seriously jeopardizes human health [6]. Within this context, the advanced oxidation processes (AOPs) have been positioned as very powerful mitigation measures, as they have been proven capable to eliminate water pollutants due to their great ability for in-situ production of strong oxidants like reactive oxygen species (e.g., hydroxyl radical ($^{\bullet}OH$)) and sulfate or chlorine radicals [4,5].

Among the AOPs, electrochemical Fenton-based technologies like electro-Fenton (EF) and photoelectro-Fenton (PEF) display unique features that confer substantial advantages in practice [7-11]. First, the use of electrocatalytic cathode materials allows the production of hydrogen peroxide from oxygen reduction reaction (ORR) (1), with two key characteristics: on site and on demand, by simply modulating the applied current or potential [12-14]. Although H_2O_2 mostly behaves as a mild oxidant against organic pollutants, it can be readily activated in the presence of iron catalyst according to Fenton's reaction (2), which originates the free and very reactive $^{\bullet}OH$ in the bulk solution at optimum pH ~3 [15-17]. However, the less reactive form of the catalyst (i.e., Fe^{3+}) may be gradually accumulated from reaction (2), which negatively affects the performance of EF and PEF processes [9,18]. To solve this problem, the second advantageous trait of electrochemical systems is the feasibility of electrocatalytic Fe^{2+} regeneration from reaction (3) at the cathode surface [8,19]. As a result of the H_2O_2 and Fe^{2+} co-generation, refractory TOrCs can be efficiently degraded by EF within few minutes at low input current [20-22]. Nonetheless, if reaction (3) is not fast enough, stable Fe(III)-carboxylate complexes can be formed [8], which is detrimental because they block the Fe^{2+} regeneration

and the organic matter mineralization. The simplest strategy to avoid the accumulation of such resistant complexes consists in the photoirradiation of the solution with UVA light, as demonstrated from the superiority of PEF over EF [14,17,23,24]. A dual mission is pursued by exposure to UVA photons: (i) photoreduce the iron-hydroxy complexes by reaction (4), which liberates the Fe^{2+} catalyst; and (ii) photodecompose the iron-carboxylate complexes by reaction (5), which enhances the total organic carbon (TOC) removal [8].

$$O_2 + 2H^+ + 2e^- \rightarrow H_2O_2 \quad (1)$$

$$Fe^{2+} + H_2O_2 \rightarrow [Fe(OH)]^{2+} + {}^{\bullet}OH \quad (2)$$

$$[Fe(OH)]^{2+} + H^+ + e^- \rightarrow Fe^{2+} + H_2O \quad (3)$$

$$[Fe(OH)]^{2+} + h\nu \rightarrow Fe^{2+} + {}^{\bullet}OH \quad (4)$$

$$[Fe(OOCR)]^{2+} + h\nu \rightarrow Fe^{2+} + CO_2 + R^{\bullet} \quad (5)$$

As can be deduced from the above description, the cathode is the most relevant component of the electrochemical cell to run EF and PEF treatments. Consequently, considerable attention has been paid to the development and modification of cathode materials. Different types of carbons, from particle beds to 3D (i.e., porous) fabrics and nanosized materials, have been widely employed as electrocatalysts due to their excellent trade-off between cost and performance, especially regarding their acceptable durability under cathodic polarization [25,26]. Many authors have employed a cell configuration in which the carbonaceous cathode is immersed into the solution, thus enabling the dissolved O_2 reduction from reaction (1) [12,18,27,28]. Despite its simplicity, the low O_2 solubility in water limits the H_2O_2 productivity, unless more complex designs are developed [29]. Alternatively, the use of the so-called air-diffusion electrode (ADE) configuration significantly upgrades the H_2O_2 electrosynthesis, thanks to the unlimited supply of atmospheric O_2 through a gas-diffusion layer (GDL) [30,31], thus being favorable to run the EF and PEF processes.

The latest trends to improve the ADE performance regard different aspects of the catalytic layer (CL): (i) development of ADEs with well-balanced hydrophilicity and aerophilicity, which contributes to confer sufficient waterproofing and reach higher O_2 utilization efficiency [32]; (ii) derived from the former, the concept of superhydrophobic CL has given rise to electrodes that operate under natural air diffusion (so-called NADEs), which allows avoiding the need of an air pump [21,33,34]; and (iii) the modification of carbons for the CL, either by enriching the surface chemistry with heteroatoms like N [24], enhancing the textural properties [14] or doping with quinones [35], metal nanoparticles [36,37] or even single atom catalysts [38]. In contrast, much less attention has been paid to the effect of the substrate where the CL is deposited. Carbon cloth (C_{cloth}) and carbon paper are the most common substrates to prepare ADEs for EF and PEF, acting as GDL at the same time [14,15,20,24,37,39]. Nonetheless, C_{cloth} is much less conductive than metal substrates, which can induce certain ohmic drop especially in low conductive media, thus shifting the cathodic potential toward less favorable values for reactions (1) and (3). Furthermore, the stability of the carbon support is expected to drop at industrial-relevant current values [40]. Additionally, despite the current technological maturity of ADEs, their relatively low pressure resistance may cause cathode flooding during long term operation, thus resulting in deactivation. Aiming to address these potential drawbacks, some authors have replaced the GDL-CL ensemble by a so-called conductive catalytic layer (CCL) composed of a metallic mesh, which acts as electric and mechanical support, coated with a carbon + polymer mixture in which the ORR (1) takes place. Stainless steel (SS_{mesh}) is often chosen for CCL configuration [17,41-43], although this material poses some risks associated to its instability in acid medium. Ti_{mesh} coated with carbon black-PTFE has also shown a good ability for H_2O_2 electrogeneration and removal of phenol under EF conditions [35]. The use of Ni_{mesh} seems a better choice because long-term stability (> 85% efficiency) with low energy consumption (< 10 kWh (kg H_2O_2)$^{-1}$) has been reported for H_2O_2 production using a Ni_{mesh}|carbon black-PTFE

cathode in the context of decentralized wastewater treatment [13], whereas up to 70% efficiency for H_2O_2 accumulation has been described using a Ni_{mesh}|mesoporous carbon-PTFE cathode [44]. A more complex cathode composed of Ni_{mesh}|reduced graphene oxide|graphene-PTFE has shown an excellent H_2O_2 production without apparent corrosion, allowing total degradation of 50 mL of 20 mg L^{-1} Rhodamine B with 0.05 M Na_2SO_4 in only 60 min under optimum conditions of 0.3 mM Fe^{2+}, pH 3.0 and 20 mA cm^{-2} [45]. Unfortunately, the behavior of a Ni_{mesh} support in ADEs has not been explored yet for application in PEF.

The main goal of this work is to ascertain if Ni_{mesh} could really become advantageous as support over the more ubiquitous C_{cloth} and SS_{mesh} for H_2O_2 production with ADEs, as we are not aware of such a comparison in the literature. Once confirmed this hypothesis, acidic solutions of the penicillin-class antibiotic carbenicillin (CBN) have been systematically treated by EF and PEF for the first time, using both model solutions and actual urban wastewater. Note that CBN-resistant bacteria have been detected in treated wastewater effluents [46], thereby corroborating the urgency for more powerful methods to remove antibiotics from water.

2. Materials and methods

2.1. Chemicals

Commercial carbenicillin disodium salt (M = 422.36 g mol^{-1}) of analytical grade (89.0-100.5%) was purchased from Sigma-Aldrich and did not require further purification. Salts used for the preparation of water matrices (Na_2SO_4, K_2SO_4, NaCl, $NaNO_3$ and $NaHCO_3$) were of analytical grade (> 99.0% purity) obtained from Panreac, Prolabo and Probus. $FeSO_4 \cdot 7H_2O$ (99.5%) used as catalyst was supplied by J.T. Baker. Solutions to carry out the analyses and some of the water matrices tested as reaction medium for the electrolysis were prepared with pure and high-resistivity Millipore Milli-Q water (> 18.2 MΩ cm). The initial pH of all solutions was adjusted to 3.0 employing an analytical grade sulfuric acid solution (95-97%)

purchased from Merck. All the other chemicals needed for the work were of analytical or liquid chromatography grade acquired from Merck, Sigma-Aldrich and Panreac.

2.2. Aqueous matrices to run the electrolytic trials

Three different aqueous matrices have been employed for the electrolysis:

(i) An effluent collected from the secondary decanter of a WWTP located in Gavà-Viladecans (Barcelona, Spain). The total sample volume was refrigerated at 4 ºC immediately after collection. Its characteristics were measured before running the experiments: pH = 7.5, specific conductivity = 1.7 mS cm^{-1} and TOC content = 13.0 mg L^{-1}. It also contained some cations and anions such as Fe^{2+} (0.003 mM), Mg^{2+} (1.51 mM), Ca^{2+} (2.48 mM), K^{+} (1.26 mM), Na^{+} (14.26 mM), NO_2^- (0.09 mM), NO_3^- (0.27 mM), Cl^- (13.52 mM) and SO_4^{2-} (13.09 mM);

(ii) a simulated water matrix mimicking the actual effluent, which was prepared with Milli-Q water without any organic matter, attaining the following composition: 13.0 mM NaCl + 13.0 mM Na_2SO_4 + 0.60 mM K_2SO_4 + 0.30 mM $NaNO_3$ + 0.60 mM $NaHCO_3$. The solution had pH = 7.1 and conductivity = 1.8 mS cm^{-1};

(iii) solutions of 0.010 and 0.050 M Na_2SO_4 in Milli-Q water at pH = 7.0 with conductivity of 1.8 and 6.9 mS cm^{-1}, respectively, used for comparison.

Prior to the electrolytic assays, all the solutions were acidified to pH 3.0 with H_2SO_4 solution since this is the optimum value for the EF and PEF processes. The solution conductivity did not change substantially. In CBN degradation trials, the solution pH was not regulated because it slowly dropped down to final values near 2.7-2.8. This acidification can be related to the formation of acidic byproducts, as will be discussed below.

2.3. Preparation of air-diffusion electrodes

In all cases, 0.20 g of carbon black (Cabot Corporation), 0.15 mL of 60% (w/w) polytetrafluoroethylene (PTFE) dispersion (Sigma-Aldrich) and 20 mL ethanol (Panreac) were introduced in a small beaker and vigorously mixed in an ultrasonic bath (Selecta) for 30 min.

156 The obtained dispersion was heated at 80 ºC until it turned into an ointment, which was put
157 onto the substrate with a brush. The substrate was an SS_{mesh}, Ni_{mesh} or C_{cloth} (Goodfellow and
158 BASF), all with dimensions of 5.0 cm × 6.0 cm and previously cleaned with 3 M HCl. The
159 SS_{mesh} had 0.066 mm wire diameter, 0.103 mm nominal aperture, 150 × 150 wires per inch and
160 0.132 mm thickness, whereas the Ni_{mesh} had 0.011 mm wire diameter, 0.04 mm nominal
161 aperture, 500 wires per inch and 0.004 mm thickness. The supported mixtures were then
162 submitted to a pressure of 2 tons in a hydraulic press (Cortazar, No. 2038) at room temperature
163 for 30 min, and further calcined in a muffle furnace at 360 ºC for 30 min. Once the resulting
164 materials reached ambient temperature, they were cut into circles of ~2 cm diameter (3 cm^2
165 area) and placed into cylindrical polypropylene holders to finally obtain the SS_{mesh}|C-PTFE,
166 Ni_{mesh}|C-PTFE and C_{cloth}|C-PTFE ADEs that were employed as cathodes in the electrolytic
167 experiments.

168 *2.4. Experimental setup*

169 Direct photolysis, anodic oxidation with cathodic H_2O_2 production (AO-H_2O_2), EF and
170 PEF treatments of the drug solutions were carried out in an undivided cylindrical glass cell that
171 had a jacket to recirculated external thermostated water at 25 ºC. Solutions of 150 mL were
172 treated under fast stirring with a magnetic follower. The cell contained one anode, which
173 consisted in either a pure Pt sheet (SEMPSA) or a boron-doped diamond (BDD) thin film coated
174 on a Si wafer (NeoCoat), and one cathode consisting of a polypropylene tube with the ADE
175 placed at the bottom. One of the three ADEs manufactured as explained above was used as the
176 cathode, fed with air from a pump to ensure a flow rate of 0.6 L min^{-1} for H_2O_2 production. The
177 geometric area of all the electrodes was 3 cm^2, being the anode and the tubular plastic holder
178 containing the cathode placed in parallel at an interelectrode distance of 1 cm. The
179 electrochemical runs were performed at constant current (*I*) supplied by an Amel 2049
180 potentiostat-galvanostat. The cell voltage (E_{cell}) was monitored on a Demestres 601BR digital

multimeter. The electrodes were cleaned before each trial by means of a 180-min polarization in 0.050 M Na_2SO_4 at I = 300 mA. The Fe^{2+} catalyst concentration in EF and PEF was 0.50 mM, as it was found optimal in previous works at acid pH [20]. The PEF assays were made by exposing the solution to a 6 W Philips fluorescent black light blue lamp, which irradiated UVA light (λ_{max} = 360 nm, power density = 5 W m^{-2}) from 7 cm over the liquid surface. The photolytic experiments were performed under analogous conditions, but without supplying current to the electrodes.

2.5. Analytical methods

Scanning electron microscopy (SEM) images and energy dispersive X-ray spectroscopy (EDS) data to assess the morphological characteristics and surface composition of the as-prepared and used Ni_{mesh}|C-PTFE ADEs were obtained with a JEOL field-emission microscope (FESEM) JSM-7100F operating at 15 kV, equipped with an INCA analyzer.

A Metrohm 644 conductometer and a Crison GLP 22 pH-meter were used to monitor the electrical conductance and pH of the aqueous solutions, respectively. Upon collection, the samples were filtered with Whatman 0.45 μm PTFE filters to preserve the instruments and avoid false readings. The concentration of anions and cations like NH_4^+, Fe^{2+}, Fe^{3+} or total iron, as well as that of H_2O_2 and active chlorine, were determined following the procedures described elsewhere [30]. The $^{\bullet}OH$ concentration was quantified replacing the pollutant by analytical grade dimethylsulfoxide (DMSO, Sigma-Aldrich) at a concentration of 250 mM [47].

Acute toxicity of samples collected before and after treatment of 0.0490 mM CBN solutions in the secondary WWTP effluent was determined via the Microtox method by measuring the EC_{50} value of bioluminescence of the marine bacteria *Vibrio fischeri*. An AutolumatPlus LB 953 luminometer from Berthold (Pforzheim, Germany) was used, following the international procedure OIN 11348-3. The bioluminescence intensity of samples was measured both, at 5 and 15 min of exposure at 15 °C.

206 Reversed-phase and ion-exclusion high-performance liquid chromatography (HPLC) were
207 used to quantify CBN and the generated carboxylic acids, respectively. In EF and PEF, the
208 microfiltered samples were temporarily stored with addition of acetonitrile (1:1 in volume),
209 aiming to scavenge the residual oxidants in solution. In both methods, 10 μL aliquots were
210 injected into a Waters 600 liquid chromatograph connected to a Waters 996 PDA detector,
211 which was set at λ = 220 nm for CBN and λ = 210 nm for carboxylic acids. The reversed-phase
212 HPLC analysis was carried out using a BDS Hypersil C18 (250 mm × 4.6 mm) column at room
213 temperature and a 40:60 (v/v) acetonitrile/water (10 mM KH_2PO_4 at pH 3.0) mixture as the
214 mobile phase at 1.0 mL min^{-1}. An isolated peak for CBN was obtained at retention time of 4.3
215 min. The column was replaced by a Bio-Rad Aminex HPX 87H (300 mm × 7.8 mm) column
216 heated at 35 ºC for ion-exclusion HPLC analysis, being the mobile phase replaced by a 4 mM
217 H_2SO_4 solution eluted at 0.6 mL min^{-1}.
218 The non-purgeable organic content (NPOC) mode was used to quantify the TOC content
219 of the samples on a VCSN TOC analyzer (Shimadzu). For each measurement, the average value
220 of analyses made in triplicate with ±1% accuracy is reported. The TOC removal was readily
221 calculated from Eq. (6):

222 $$\text{TOC removal (in \%)} = \frac{(\Delta \text{TOC})_{\text{exp}}}{\text{TOC}_\text{o}} 100 \quad (6)$$

223 where $(\triangle \text{TOC})_{\text{exp}} = (\text{TOC}_0 - \text{TOC}_t)$, accounts for the TOC decay (in mg L^{-1}) as the difference
224 between the values at time 0 and *t*. The mineralization current efficiency (MCE) at given *I* (in
225 A) and *t* (in h) was determined according to the following Eq. (7) [15,20]:

226 $$\text{MCE (in \%)} = \frac{nFV_\text{s}(\Delta \text{TOC})_{\text{exp}}}{4.32x10^7 mIt} 100 \quad (7)$$

227 where F = 96,487 C mol^{-1} is the Faraday constant, V_s is the volume of treated solution (in L),
228 4.32×10^7 is a factor for unit homogenization and m = 17 is the number of carbon atoms of
229 CBN. The number of electrons exchanged per each CBN molecule was n = 74 from the

following theoretical overall mineralization reaction considering that only NH_4^+ was formed from the initial N, as will be discussed in subsection 3.7:

$$C_{17}H_{18}N_2O_6S + 32H_2O \rightarrow 17CO_2 + 2NH_4^+ + SO_4^{2-} + 74H^+ + 74e^- \quad (8)$$

The electrolytic energy consumption per unit TOC mass (EC_{TOC}), accounting only for the energy required to run the electrochemical process, was obtained as follows [15,20]:

$$EC_{TOC} \text{ (in kWh (g TOC)}^{-1}) = \frac{E_{cell} I t}{V_s (\Delta TOC)_{exp}} \quad (9)$$

where E_{cell} is in V. In the case of PEF, the $EC_{TOC,total}$ considering the energy power (P, in W) of the UVA lamp was also determined from Eq. (10):

$$EC_{TOC,total} \text{ (in kWh (g TOC)}^{-1}) = \frac{(E_{cell} I + P) t}{V_s (\Delta TOC)_{exp}} \quad (10)$$

The trials were always made at least twice, and average values are reported. Therefore, error bars referred to a 95% confidence interval are displayed in the figures.

The organic byproducts formed during the photolysis, EF and PEF treatments of CBN solutions were extracted out with CH_2Cl_2 in three times, and the obtained organic volume was further dried using anhydrous Na_2SO_4 to be subsequently reduced to about 1 mL with a gentle N_2 stream. The remaining organic phase was analyzed by GC-MS using an earlier procedure [48], with a non-polar Teknokroma Sapiens- X5ms (0.25 μm, 30 m × 0.25 mm) column, and the spectra obtained were compared with those of the NIST05 database.

3. Results and discussion

3.1. Performance of Ni_{mesh}, SS_{mesh} and C_{cloth} as substrates for ADEs

Fig. 1a and 1b highlight representative surface morphologies of the pristine Ni_{mesh}|C-PTFE ADE and the same material after being used as cathode for H_2O_2 production three consecutive runs. The carbon black nanoparticles with a size of about 100 nm are evenly distributed on the

electrode surface, and the large number of micropores and mesopores are conducive to the air penetration and the two-electron oxygen reduction reaction (1) at the solid-liquid interface. Worth noting, the surface morphology of the Ni_{mesh}|C-PTFE ADE did not change significantly after the sequential electrolytic runs. The carbon black particles remained firmly attached to the electrode surface, which provides a guarantee for the superior endurance for H_2O_2 production when Ni_{mesh} is employed as the substrate. Fig.1c depicts the elemental composition of the prepared Ni_{mesh}|C-PTFE ADE, obtained from EDS analysis, mainly showing Ni element from the mesh substrate and C element from the catalytic layer, being the content of C about 2000-fold greater, which informs about the good surface coating. Fig. 1d depicts the H_2O_2 accumulation profiles obtained in three consecutive runs with a duration of 360 min under the AO-H_2O_2 conditions described in Fig. 1b, using the Ni_{mesh}|C-PTFE ADE as cathode. The accumulated H_2O_2 concentration increased gradually in the medium due to its continuous production from reaction (1). The profiles show good reproducibility in the successive runs, attaining final values from 51.2 to 48.4 mM. This behavior denotes a good performance of the Ni_{mesh}|C-PTFE ADE, without significant loss in electroactivity, during prolonged electrolysis. To confirm this finding, a trial with a duration of 48 h at 100 mA initiated with a fresh Ni_{mesh}|C-PTFE ADE as cathode was also made, and the corresponding accumulated H_2O_2 is presented in Fig. 1e. As can be seen, a steady concentration of about 60 mM H_2O_2 was obtained from 25 h of electrolysis, i.e., time at which the rates of cathodic H_2O_2 production and destruction mainly at the anode from reaction (11) [8] became equal. The high stability of the cathode was confirmed from the low final dissolved Ni concentration, which was below the limit of detection of 0.2 mg L^{-1}. Note that an additional chemical experiment mixing a Ni(II) salt with H_2O_2 confirmed that the latter cannot be activated by this metal cation. Eq. (11) makes in evidence the generation of heterogeneous hydroperoxyl radical ($HO_2^{\bullet}$) at the anode M, a much weaker oxidant than heterogeneous $^{\bullet}OH$ that is concomitantly formed at the same anode M from water

oxidation according to reaction (12). Consequently, in the AO-H_2O_2 process, the organic pollutants are destroyed by the electrogenerated H_2O_2, heterogeneous $HO_2^{\bullet}$ and, pre-eminently, heterogeneous hydroxyl radical, being the reactions mediated by the two radicals only circumscribed to the anode surface and its vicinity.

$$M + H_2O_2 \rightarrow M(HO_2^{\bullet}) + H^+ + e^- \quad (11)$$

$$M + H_2O \rightarrow M(^{\bullet}OH) + H^+ + e^- \quad (12)$$

Comparative long-term assays for 48 h were carried out with the two other prepared ADE cathodes. Fig. S1 highlights that the use of an SS_{mesh}|C-PTFE ADE cathode led to a plateau from 35 h of electrolysis, attaining lower final H_2O_2 concentration close to 50 mM. This is indicative of a loss of stability of this cathode, which can be explained by the leaching of Fe^{2+} and other metal ions from the alloy under acidic conditions. A slight corrosion of the SS_{mesh} surface was observed by SEM after this trial, thus confirming this hypothesis. On the other hand, Fig. S1 also shows a large instability of the C_{cloth}|C-PTFE ADE, yielding a good H_2O_2 accumulation up to 40 mM in 10-22 h, but followed by a dramatic decay down to 21.5 mM. This detrimental behavior can be related to the flooding of the air chamber, which was confirmed when the cathode was disassembled after the experiment. Based on these findings, the Ni_{mesh}|C-PTFE ADE was chosen as cathode for subsequent trials to investigate the CBN removal.

3.2. Degradation of carbenicillin by electrochemical AOPs with H_2O_2 production

3.2.1. Effect of the aqueous matrix

First, the treatment of solutions with 0.0490 mM CBN in 0.010 M Na_2SO_4, simulated water or secondary WWTP at pH 3.0 and 25 ºC was addressed. Fig. 2a shows a poor degradation of the drug, reaching 13% after 20 min, by direct photolysis with UVA light in the secondary WWTP effluent. This is a clear evidence of the low photoactivity of the drug, which gives rise

to a very low mineralization (see Fig. 2b). Further studies were focused on the PEF treatment of the above solutions in the three media by adding 0.50 mM Fe^{2+} as catalyst, always irradiating with the same UVA lamp. The reactor comprised a BDD anode and a Ni_{mesh}|C-PTFE ADE as cathode, and trials were made at I = 20 mA. BDD was chosen because it is the most powerful anode to achieve the highest amount of reactive M(•OH) from reaction (12). Fig. 2a depicts that total degradation was achieved after decreasing times from 18 min in actual wastewater > 15 min in simulated water > 13 min in 0.010 M Na_2SO_4. The concentration decays obeyed a pseudo-first-order reaction and the corresponding pseudo-first-rate constant (k_1) raised from 0.157 to 0.180 min^{-1}, as shown in Table 1. This deceleration can be explained by the prevalence of less reactive oxidizing agents in the simulated matrix, owing to the formation of active chlorine (HClO) from Cl^- oxidation via reactions (13) and (14) [9,15], although it is more powerful than H_2O_2 and heterogeneous oxidizing radicals produced by reactions (11) and (12). HClO competes with the stronger homogeneous •OH formed from reactions (2) and (4), which is less abundant than in 0.010 M Na_2SO_4. Consequently, the slowest drug decay found in the secondary WWTP effluent can be ascribed to this phenomenon, in addition to the presence of organic matter that reduces the quantity of oxidants available for CBN degradation.

$$2Cl^- \rightarrow Cl_2 + 2e^- \quad (13)$$

$$Cl_2 + H_2O \rightarrow HClO + Cl^- + H^+ \quad (14)$$

The abovementioned reactivity was also verified for the normalized TOC abatement profiles, as depicted in Fig. 2b. Table 1 shows that, after 360 min, the percentage of TOC removed increased as follows: simulated water (59.6%) < urban wastewater (76.7%) < 0.010 M Na_2SO_4 (84.0%). The resulting MCE at 360 min for trials in media with the same initial TOC of 10.0 mg L^{-1} was then much greater for the sulfate medium as compared with the simulated water (i.e., 11.4% vs. 8.1%), whereas lower EC_{TOC} values were calculated in the former case.

The lower mineralization reached in the simulated water suggests the formation of more recalcitrant chlorinated derivatives, as will be discussed below. On the other hand, a good TOC elimination was achieved in the secondary WWTP effluent despite its higher initial TOC (23.0 mg L^{-1}), giving rise to a much lower EC_{TOC} (see Table 1). This positive result is indicative of a low accumulation of chlorinated derivatives from the components of the WWTP, which are preferentially mineralized.

The final concentrations of accumulated H_2O_2 and active chlorine in the PEF trials of Fig. 2b were measured. Fig. 2c reveals a greater H_2O_2 consumption in 0.010 M Na_2SO_4, as expected if it is more rapidly transformed into homogeneous $^{\bullet}OH$ from Fenton's reaction (2) thanks to the absence of active chlorine, giving rise to the fastest mineralization (see Fig. 2b). In contrast, Fig. 2c highlights that the presence of active chlorine inhibits the activation of H_2O_2, to a larger extent in the urban wastewater than in the simulated water. The larger accumulation of active chlorine in the secondary WWTP effluent informs about the relevant role of the heterogeneous BDD($^{\bullet}OH$) formed from reaction (12) to oxidize its organic components, yielding greater mineralization as depicted in Fig. 2b.

3.2.2. Effect of UVA light

The contribution of the UVA light to the high performance of the PEF process was evaluated in simulated water from comparison with the analogous EF trial. The trials were made under the same conditions described in Fig. 2a and 2b but applying a higher I = 100 mA. Fig. 3a shows the much faster total CBN removal in about 5 min obtained in PEF at such higher current, owing to the acceleration of reactions (1), (12) and (13) that causes: (i) a quicker production of H_2O_2, originating more homogeneous $^{\bullet}OH$ from Fenton's reaction (2) and photolytic reaction (4), as well as a greater amount of (ii) heterogeneous BDD($^{\bullet}OH$) and (iii) active chlorine. In contrast, the EF treatment at I = 100 mA led to overall drug abatement in a longer time of 7 min. The enhancement of CBN removal in the PEF treatment can be related to

the additional production of homogeneous •OH upon action of UVA light from the photolytic reaction (4). This positive effect of irradiation can be better observed in Fig. 3b, where a quicker TOC decay occurred in PEF, finally attaining 86.5% mineralization, much higher than 66.0% found in EF. Apart from the larger production of homogeneous •OH from reaction (4), the greater mineralization achieved in PEF can be attributed to the photolysis of Fe(III)-carboxylate complexes via reaction (5), favoring the destruction of the final carboxylic acids. Table 1 makes in evidence the superior efficiency of PEF over EF, associated with a lower EC_{TOC} in the former case if the energy consumption of the UVA lamp is not considered. This is an apparent drawback in practice, since it can be solved by using free and renewable sunlight as energy source in the so-called solar PEF (i.e., SPEF) process. The larger mineralization by PEF presupposes a greater consumption of generated oxidants, i.e., H_2O_2 and active chlorine. This behavior was confirmed by monitoring the evolution of these species during the electrolysis, as presented in Fig. 3c and 3d, respectively. Smaller concentrations of H_2O_2 (20.3 vs. 28.5 mM) and active chlorine (0.86 vs. 1.28 mM) were accumulated after 360 min of PEF as compared to EF, in agreement with its higher oxidation power. Note that 51.2 mM H_2O_2 was produced in the system under comparable AO-H_2O_2 conditions (see Fig. 1d). This means that 27.7 mM H_2O_2 (54.1% of the initially accumulated) was consumed to form •OH from Fenton's reaction (2) by EF, whereas about 30.9 mM H_2O_2 could not be accumulated in PEF (this accounts for 60.3% as compared with AO-H_2O_2 data. The H_2O_2 activation was 6.2% larger than that reached by EF due to the production of •OH from Fenton's reaction (2), further accelerated by the additional Fe^{2+} photoregeneration.

3.2.3. Effect of the anode and applied current

The influence of other key experimental variables like the anode used and the applied *I* was comparatively studied in the secondary WWTP effluent by means of AO-H_2O_2, EF and PEF. These runs were carried out with a given composition of the CBN solution by using a Pt or

BDD anode and a Ni_{mesh}|C-PTFE ADE as cathode, at *I* values of 10, 20 and 100 mA. Fig. 4a highlights for AO-H_2O_2 process with BDD a more rapid drug abatement with increasing *I*, disappearing in 40 min at 10 mA, 35 min at 20 mA and 25 min at 100 mA, as result of the progressively greater generation of H_2O_2 from reaction (1), heterogeneous BDD($HO_2^{\bullet}$) from reaction (11), heterogeneous BDD($^{\bullet}OH$) from reaction (12) and active chlorine from reactions (13) and (14). A slower CBN decay leading to total removal in 30 min can be observed in Fig. 4a when using Pt at *I* = 100 mA. This agrees with the expected lower oxidation ability of generated heterogeneous Pt($^{\bullet}OH$) as compared to that of BDD($^{\bullet}OH$) [9,20], thus confirming the positive oxidative action of the latter radical on CBN. The k_1-values determined for these assays are collected in Table 1, increasing from 0.017 to 0.064 min^{-1} using BDD at rising *I* from 10 to 100 mA, being 0.055 min^{-1} when employing Pt at *I* = 100 mA. The same tendency was obtained for the normalized TOC removal, as can be seen in Fig. 4b, in agreement with the relative oxidation power. The highest mineralization of 37.5% was then achieved with BDD at *I* = 100 mA, decreasing down to 11.6% at *I* = 10 mA, whereas only 22.2% was achieved with Pt at *I* = 100 mA due to the poorer destruction of the organic pollutants of the WWTP by the less potent Pt($^{\bullet}OH$). This was also reflected in the corresponding EC_{TOC} values that raised from 0.554 to 9.14 kWh $(g\ TOC)^{-1}$ using BDD when *I* grew from 10 to 100 mA, as a result of the increased E_{cell}. A higher value of 13.5 kWh $(g\ TOC)^{-1}$ was calculated for Pt at *I* = 100 mA due to the much lower TOC decay. Using the BDD anode, the final accumulated H_2O_2 and active chlorine concentrations decayed as the applied *I* was diminished (see Fig. 4c) because of their lower generation; this, alongside the production of less heterogeneous BDD($^{\bullet}OH$), explains the poorer degradation. Fig. 4c also reveals the greater H_2O_2 accumulation when BDD was replaced by Pt, at *I* = 100 mA, indicating that the oxidation of this species to $HO_2^{\bullet}$ is not as remarkable as in the case of BDD. In contrast, more active chlorine was formed and accumulated with

399 BDD, according to the greater oxidation of chloride. All these findings allow inferring that
400 BDD is suitable as the anode in the AO-H_2O_2 process.

401 When the EF process was investigated in detail, quicker degradation and mineralization of
402 the drug was observed, being attributed to the production of the strong homogeneous $^{\bullet}OH$ from
403 Fenton's reaction (2). The oxidative action of this radical is well proven from the results given
404 in Fig. 5a and 5b. The normalized CBN concentration dropped down more rapidly with BDD
405 when *I* increased from 10 to 100 mA, with total abatement at gradually shorter time from 21 to
406 7 min (see Fig. 5a), as expected from the larger generation of oxidants (mainly heterogeneous
407 BDD($^{\bullet}OH$), homogeneous $^{\bullet}OH$ and HClO). The k_1-values were higher than those obtained in
408 AO-H_2O_2, increasing from 0.057 to 0.413 min^{-1} (see Table 1). The same trend can be observed
409 in Fig. 5b for TOC decay, which reached 40.8%, 53.6% and 66.9% after 360 min of treatment
410 at 10, 20 and 100 mA, respectively. Moreover, EC_{TOC} was increased from 0.158 to 5.10 kWh
411 $(g\ TOC)^{-1}$ (see Table 1) due to the gradual increase of E_{cell} and the loss of current efficiency.
412 Fig. 5a depicts a similar degradation rate of the drug with Pt and BDD at I = 100 mA, with a
413 similar k_1-value (see Table 1). This indicates that homogeneous $^{\bullet}OH$ is the main oxidant. In
414 contrast, TOC was more slowly reduced with Pt, only reaching 50.8% in 360 min (see Fig. 5b),
415 with a higher EC_{TOC} = 5.89 kWh $(g\ TOC)^{-1}$ (see Table 1). These findings corroborate the
416 superiority of EF with BDD by the larger destruction of the reaction byproducts and the other
417 organic components of the WWTP effluent by heterogeneous BDD($^{\bullet}OH$), as stated above for
418 the AO-H_2O_2 process.

419 The PEF process was the most powerful treatment to decontaminate the secondary WWTP
420 effluent with spiked CBN. Fig. 6a shows the expected faster abatement of the drug at shorter
421 times with rising *I* between 10 and 100 mA using BDD, obtaining a similar rate with this anode
422 and Pt at I = 100 mA. The k_1-values determined in these runs were greater than those of EF (see
423 Table 1). This behavior can be again ascribed to the preferential oxidation of the drug with

homogeneous •OH and the photolytic reaction (4). The abundance of oxidants in PEF justifies its superiority with respect to all other methods. The TOC profiles were similar to those of EF but with higher removal percentages, as shows Fig. 6b, thanks to the contribution of photolysis of the final Fe(III)-carboxylate species from reaction (5). The highest TOC abatement of 86.5% was found operating with BDD at I = 100 mA, giving rise to an EC_{TOC} of 3.94 kWh (g TOC)$^{-1}$ without considering the irradiation power and 16.02 kWh (g TOC)$^{-1}$ when this parameter was included (see Table 1). The trends of the final accumulated H_2O_2 and active chlorine in the PEF assays given in Fig. 6c resembles that determined in AO-H_2O_2 (see Fig. 4c). Nevertheless, smaller values of both oxidants were obtained due to their quicker consumption under PEF conditions by the action of Fe^{2+} and UVA light. These excellent results open the door for the scale-up of the PEF treatment of urban wastewater contaminated with CBN using BDD anode and Ni_{mesh}|C-PTFE ADE as cathode, although replacing the current photoreactor by a solar photoreactor to avoid the energy penalty associated to the UV lamp.

For comparison, Table 2 shows selected results reported in the literature for the removal of various organic pollutants by PEF with different ADEs. Note that, under analogous experimental conditions, the N_{imesh} support leads to better oxidation performance, particularly for the treatment of secondary WWTP effluents.

3.3. Time course of key species and reaction progress

3.3.1. Profile of •OH

The production of heterogeneous M(•OH) and homogeneous •OH during the various treatments was assessed by establishing their accumulation profiles when reacting with DMSO. Fig. 7a reveals a very weak accumulation of Pt(•OH) up to 35.3 μM in simulated water when Pt was used in AO-H_2O_2 for 360 min at I = 100 mA, being vastly surpassed using the BDD anode (123.3 μM of BDD(•OH)). These findings justifies the superiority of BDD to destroy organics in AO-H_2O_2, as is shown in Fig. 4a and 4b in the case of CBN. The production of

449 homogeneous •OH was then explored by EF and PEF after adding 0.50 mM Fe^{2+} to the
450 secondary WWTP effluent using BDD for 360 min at *I* = 100 mA. As can be seen in Fig. 7a,
451 up to 301.7 μM of •OH was determined in EF, mainly due to the production of homogeneous
452 •OH from Fenton's reaction (2). Higher accumulation of •OH up to 558.0 μM was found in PEF
453 as result of the photolytic reaction (4). This agrees with the superior performance of PEF over
454 EF for CBN degradation and mineralization (see Figs. 3, 5 and 6).

455 *3.3.2. Evolution of iron species*

456 The evolution of the iron ions during the above PEF run is presented in Fig. 7b. The initial
457 0.50 mM Fe^{2+} dramatically decayed for 30 min, ending in a quasi-steady concentration of about
458 0.015 mM from 120 min of electrolysis. Despite this low residual Fe^{2+} content, the results of
459 Fig. 7a for the analogous EF process indicate that the system was able to continue generating
460 homogeneous •OH from Fenton's reaction (2) to oxidize organic pollutants. The Fe^{3+}
461 concentration originated from the Fe^{2+} transformation decayed rapidly, since the UVA lamp
462 was unable to completely photoreduce the Fe(III) species due to its limited power. As a result,
463 it reached a minimal of 0.083 mM at 90 min, whereupon it raised up to 0.20 mM at 180 min.
464 The Fe^{3+} content decay up to 90 min suggests the precipitation of $Fe(OH)_3$ onto the alkalinized
465 cathode surface, as a result of its low ability to reduce Fe^{2+} via reaction (3). Note that, although
466 part of Fe^{3+} could also be complexed by the generated final carboxylates (see subsection 3.7).
467 The further Fe^{3+} concentration increase can be ascribed to the partial redissolution of $Fe(OH)_3$
468 by the continuous acidification of the medium to pH 2.7 making the cathode surface less
469 alkaline. Note that the presence of dissolved carboxylates (see subsections below) may also
470 facilitate such redissolution. This favors the partial regeneration of Fe^{2+} and the rise of the total
471 dissolved iron concentration at times from 120 min (see Fig. 7b).

3.3.3. Evolution of the acute toxicity

The acute toxicity profile in the secondary WWTP effluent was determined from the term EC_{50}, which was determined from Microtox analysis with the marine bacteria *Vibrio fischeri*. Fig. 7c exemplifies the change of EC_{50} in this medium with 0.049 mM CBN upon PEF treatment with BDD at *I* values of 20 and 100 mA. The wastewater became more toxic during the first 120 and 60 min of electrolysis at such applied current, respectively, as expected if toxic byproducts derived from the drug and the other organic pollutants are formed. At longer time, the acute toxicity gradually decreased and the corresponding EC_{50} raised more quickly at 100 mA because toxic pollutants were more rapidly removed by the larger amounts of generated oxidants (see Fig. 6b). One can then infer that the decontamination by PEF process allows an efficient detoxification of the wastewater, recovering the EC_{50} value that is characteristic for the urban wastewater before spiking the antibiotic.

3.3.4. Quantification of final carboxylic acids and released inorganic ions

Depending on the experimental conditions tested, up to six short-chain linear carboxylic acids, namely α-ketoglutaric, succinic, oxaloacetic, fumaric, oxalic, and oxamic (labelled as compounds **44**-**49**, respectively), were identified by ion-exclusion HPLC analysis of the treated solution initially containing 0.0490 mM drug in simulated water. Fig. 8a shows that direct photolysis originated a fast accumulation of acids **44** and **49** up to about 1.0 and 0.1 mg L^{-1} at 90 min, respectively, followed by their complete destruction in 180 min. When the EF process was tested with BDD at *I* = 20 mA, acids **46, 48** and **49** were more extensively formed, alongside a small amount of the acid **47**, owing to the main oxidation of more complex byproducts with $^{\bullet}OH$. Fig. 8b discloses the maximum accumulation of the three first acids between 120 and 180 min with respective contents of 1.3, 2.3, and 1.0 mg L^{-1}. In contrast, the acids **46** and **48** practically disappeared at 480 min because their Fe(III) complexes were slowly oxidized at the anode or with $^{\bullet}OH$. Compound **49** was much more recalcitrant and it attained a final content of

0.8 mg L^{-1} due to the large stability of Fe(III)-oxamate species. The analogous PEF treatment generated the acids **45**-**49**, with predominance of the acid **47** that was accumulated up to 6.4 mg L^{-1} at 120 min. Fig. 8c depicts that all these acids were completely destroyed approximately at 360 min due to the quick photolysis of their Fe(III) complexes via reaction (5), except the Fe(III)-oxamate species that were quite photostable leading to a final concentration of 0.55 mg L^{-1} of compound **49**. These results confirm the high oxidation power of PEF to remove all generated carboxylic acids formed upon reaction with •OH, only remaining the most recalcitrant Fe(III) complex of oxamic acid but at low content.

Analysis of inorganics ions during the above trials only allowed detecting the release of NH_4^+, thus confirming the reaction (8) proposed for the overall CBN mineralization. No accumulation of NO_3^- nor NO_2^- was found in the reaction media. Fig. 8d highlights that NH_4^+ reached a quasi-steady concentrations around 0.08, 0.90, and 1.20 mg L^{-1} after 360 min of direct photolysis, EF and PEF, respectively, corresponding to a loss of 0.47%, 5.1%, and 6.8% of the initial N content of CBN. The low generation of NH_4^+ in these processes suggests that a large proportion of recalcitrant N-derivatives, including oxamic acid, remains in the final treated solutions, accounting for the residual TOC.

3.4. Reaction pathways for carbenicillin mineralization

Table S1 collects the 19 aromatics, 4 heteroaromatics, 9 chloroaromatics, 9 non-carboxylic aliphatics (two of them chlorinated) and 1 short-chain linear carboxylic acid detected by GC-MS during the photolysis, EF with BDD and PEF with BDD treatments of solutions of 150 mL containing 0.0490 mM CBN (**1**) in simulated water, along with those from PEF treatment with BDD in the secondary WWTP effluent, always at pH 3.0, 25 ºC and I = 20 mA. The chloro-derivatives were only detected in the latter case, as a result of the attack of active chlorine over the organic components of the wastewater, which probably produced chlorine radicals. The non-halogenated derivatives formed under all conditions are then originated from the oxidation

mainly with •OH. Note that only compounds **7** (phenylpropanedioic acid) and **11** (benzeneacetamide) have been previously reported for the degradation of CBN, employing Cu(III) periodate complex [49] and UV/peroxydisulfate [50], respectively.

Based on the byproducts of Table S1 and the 6 final carboxylic acids identified by ion-exclusion HPLC, the routes for mineralization of **1** upon the action of •OH are proposed in Fig. 9. Up to 8 parallel paths can be observed coming from the partial or total release of the 3,3-dimethyl-7-oxo-4-thia-1-azabicyclo[3.2.0]heptane-2-carboxylic acid group of **1**, giving rise to the carboxy[(phenyl)acetyl]amino derivative to be oxidized. The decarboxylation of this byproduct yields the compound **2**, whereas the further attack of sulfo radicals originates the compound **3**, which is deaminated to the compound **8**. Other 4 primary byproducts, compounds **4** to **7**, were also formed. Further decarboxylation of compound **4** gives compound **9**, followed by its hydroxylation to produce the compound **10** that yields the compound **11** by loss of the $CH_2(OH)$ group. Oxidation of compound **5** with loss of H_2O leads to the compound **12**, which is subsequently hydroxylated to the compound **13**. The compound **6** evolves to the compound **14** that is either hydroxylated on the *p*-position of the benzene ring to form the compound **15** or over the carbonyl group to give the aromatic carboxylic acid **16**. Hydroxylation on the *o*-position of the benzene ring of **16** produces the compound **17**. The compound **7** undergoes total decarboxylation to generate the compound **18** that evolves to compounds **19** and **20** via hydroxylation with oxidation and decarboxylation, respectively. The carboxy[(phenyl)acetyl]amino derivative can also suffer cyclization to form the heteroaromatics **21** and **22**. Consecutive hydroxylation with oxidation of **21** leads to the compounds **23** and **24**. The benzene cleavage of the above aromatic and heteroaromatic byproducts gives: (i) a mixture of 7 aliphatics, compounds **34** to **40**, being noticeable that either the release of a cyanide group of **34** or the hydroxylation with oxidation of **35** yields the compound **40**, and (ii) a mixture of 7 short-chain linear carboxylic acids, compounds **41** and **44**

547 to **49**, where oxalic (**48**) and oxamic (**49**) acids are ultimate carboxylic acids that can be directly
548 converted into CO_2 [7,8].

549 Fig. 10 presents the proposed routes for the formation of chloro-derivatives by PEF with
550 BDD in the secondary WWTP effluent. It is assumed that they are generated from the
551 consecutive action of $^{\bullet}OH$ and HClO (or chlorine radicals produced from it). Chlorination over
552 either the –OH group or the *p*-position of the benzene ring of **16** gives the chloroaromatics **25**
553 or **26**, respectively. Compound **18** can undergo dechlorination to form the compound **27** or
554 chlorination with methylation to give the compound **28**. Subsequent chlorination over the *m*-
555 position of the benzene ring or the lateral methyl group of the latter byproduct yields the
556 chloroaromatics **29** or **30**, respectively. Chlorination of the –OH group of **19** leads to the
557 generation of compound **31**. *p*-Chlorination of the benzene ring of some aromatics also yields
558 the chloroaromatics **32** and **33**. Finally, the benzene cleavage of the above chloroaromatics
559 gives rise to the chloroaliphatics **42** and **43**.

560 **4. Conclusions**

561 It has been shown that the Ni_{mesh}|C-PTFE ADE is a more stable cathode than alternative
562 SS_{mesh}|C-PTFE and C_{cloth}|C-PTFE ADEs, as evidenced from the greater endurance to produce
563 H_2O_2 for 48 h. CBN is scarcely removed by direct UVA photolysis. In contrast, the PEF
564 treatment in different water matrices with a BDD anode and a Ni_{mesh}|C-PTFE ADE as cathode
565 leads to total drug removal, which is decelerated in the order: sulfate medium > simulated water
566 > urban wastewater. Similarly, much faster mineralization occurs in sulfate medium than in the
567 other two media. The degradation profiles have been correlated with the different accumulation
568 of H_2O_2, active chlorine and hydroxyl radicals over time. The drug decays always obeys a
569 pseudo-first-order kinetics. In the secondary WWTP effluent, the CBN oxidation is faster as *I*
570 is risen, but with higher EC_{TOC}, following the sequence: AO-H_2O_2 < EF < PEF, and BDD was
571 superior to Pt anode in all processes. Fe^{3+} formed from Fenton's reaction (2) partially

precipitates as $Fe(OH)_3$ onto the cathode surface at the beginning of the treatments, further being slowly redissolved when the medium becomes slightly acidified. Since the PEF process is too expensive due to the energy consumption from the UVA lamp, SPEF is proposed as a potentially viable method in practice. Based on the 48 byproducts detected by GC-MS and ion-exclusion HPLC analyses of treated solutions, two reaction sequences for CBN mineralization involving oxidation with •OH alone and combined with active chlorine are finally proposed.

Acknowledgments

The authors are grateful for the financial support from projects 19PTZWHZ00050 (Tianjin Science and Technology Program, China), 22106036 and 52170085 (National Natural Science Foundation of China) and PID2019-109291RB-I00 (MCIN/AEI/10.13039/501100011033, Spain), as well as for the PhD scholarship awarded to Gengbo Ren (State Scholarship Fund, CSC, China).

References

[1] Y. Wen, G. Schoups, N. van de Giesen, Sci. Rep. 7 (2017) 43289. https://doi.org/10.1038/srep43289

[2] R. Naidu, B. Biswas, I.R. Willett, J. Cribb, B. Kumar Singh, C. Paul Nathanail, F. Coulon, K.T. Semple, K.C. Jones, A. Barclay, R. John Aitken, Environ. Int. 156 (2021) 106616. https://doi.org/10.1016/j.envint.2021.106616

[3] R. Fuller, P.J. Landrigan, K. Balakrishnan, G. Bathan, S. Bose-O'Reilly, M. Brauer, J. Caravanos, T. Chiles, A. Cohen, L. Corra, M. Cropper, G. Ferraro, J. Hanna, D. Hanrahan, H. Hu, D. Hunter, G. Janata, R. Kupka, B. Lanphear, M. Lichtveld, K. Martin, A. Mustapha, E. Sanchez-Triana, K. Sandilya, L. Schaefli, J. Shaw, J. Seddon, W. Suk, M.M. Téllez-Rojo, C. Yan, Lancet 6 (2022) e535-e547. https://doi.org/10.1016/S2542-5196(22)00090-0

[4] M. Zahir Akbari, Y. Xu, Z. Lu, L. Peng, Environ. Adv. 5 (2021) 100111. https://doi.org/10.1016/j.envadv.2021.100111[5] D.B. Miklos, C. Remy, M. Jekel, K.G. Linden, J.E. Drewes, U. Hübner, Water Res. 139 (2018) 118-131. https://doi.org/10.1016/j.watres.2018.03.042

[6] C. Mutuku, Z. Gazdag, S. Melegh, World J. Microbiol. Biotechnol. 38 (2022) 152. https://doi.org/10.1007/s11274-022-03334-0

[7] H. Monteil, Y. Péchaud, N. Oturan, M.A. Oturan, Chem. Eng. J. 376 (2019) 119577. https://doi.org/10.1016/j.cej.2018.07.179

[8] I. Sirés, E. Brillas, Curr. Opinion Electrochem. 27 (2021) 100686. https://doi.org/10.1016/j.coelec.2020.100686

[9] E. Brillas, Sci. Total Environ. 819 (2022) 153102. https://doi.org/10.1016/j.scitotenv.2022.153102

[10] H. Kadji, I. Yahiaoui, Z. Garti, A. Amrane, F. Aissani-Benissad, Chinese J. Chem. Eng. 32 (2021) 183-190. https://doi.org/10.1016/j.cjche.2020.08.032

[11] H. Kadji, I. Yahiaoui, F. Akkouche, F. Boudrahem, S. Ramdani, A. Saidane, A. Manseri, A. Amrane, F. Aissani-Benissad, Water Sci. Technol. 85 (2022) 1840-1854. doi: 10.2166/wst.2022.078

[12] G. Ren, M. Zhou, P. Su, W. Yang, X. Lu, Y. Zhang, J. Hazard. Mater. 368 (2019) 830-839. https://doi.org/10.1016/j.jhazmat.2019.01.109

[13] Y. Li, Y. Zhang, G. Xia, J. Zhan, G. Yu, Y. Wang, Front. Environ. Sci. Eng. 15(1) (2021) 1. https://doi.org/10.1007/s11783-020-1293-2

[14] Y. Zhang, G. Daniel, S. Lanzalaco, A.A. Isse, A. Facchin, A. Wang, E. Brillas, C. Durante, I. Sirés, J. Hazard. Mater. 423 (2022) 127005. https://doi.org/10.1016/j.jhazmat.2021.127005

[15] G. Coria, T. Pérez, I. Sirés, E. Brillas, J.L. Nava, Chemosphere 198 (2018) 174-181. https://doi.org/10.1016/j.chemosphere.2018.01.112

[16] Q.Z. Zhang, M.H. Zhou, Z.C. Lang, X.D. Du, J.J. Cai, L.J. Han, Chem. Eng. J. 413 (2021) 127564. https://doi.org/10.1016/j.cej.2020.127564

[17] P.J.M. Cordeiro-Junior, A.S. Martins, G.B.S. Pereira, F.V. Rocha, M.A. Rodrigo, M.R.V. Lanza, Sep. Purif. Technol. 285 (2022) 120299. https://doi.org/10.1016/j.seppur.2021.120299

[18] F. Sopaj, N. Oturan, J. Pinson, F.I. Podvorica, M.A. Oturan, Chem. Eng. J. 384 (2020) 123249. https://doi.org/10.1016/j.cej.2019.123249

[19] M. Liu, Z. Feng, X. Luan, W. Chu, H. Zhao, G. Zhao, Environ. Sci. Technol. 55(9) (2021) 6042-6051. https://doi.org/10.1021/acs.est.0c08018

[20] A. Thiam, R. Salazar, E. Brillas, I. Sirés, Chem. Eng. J. 335 (2018) 133-144. https://doi.org/10.1016/j.cej.2017.10.137

[21] W. Wang, Y.C. Li, Y.W. Li, M.H. Zhou, O.A. Arotiba, Chemosphere 250 (2020) 126177. https://doi.org/10.1016/j.chemosphere.2020.126177

[22] Y. Zhu, F. Deng, S. Qiu, F. Ma, Y. Zheng, R. Lian, J. Hazard. Mater. 403 (2021) 123950. https://doi.org/10.1016/j.jhazmat.2020.123950

[23] Y. Zhang, A. Wang, S. Ren, Z. Wen, X. Tian, D. Li, J. Li, Chemosphere 221 (2019) 423-432. https://doi.org/10.1016/j.chemosphere.2019.01.016

[24] G. Daniel, Y. Zhang, S. Lanzalaco, F. Brombin, T. Kosmala, G. Granozzi, A. Wang, E. Brillas, I. Sirés, C. Durante, ACS Sustain. Chem. Eng. 8 (2020) 14425-14440. https://doi.org/10.1021/acssuschemeng.0c04294

[25] G.-L. Chai, Z. Hou, T. Ikeda, K. Terakura, J. Phys. Chem. C 121 (2017) 14524-14533. https://doi.org/10.1021/acs.jpcc.7b04959

[26] Y.-J. Wang, B. Fang, D. Zhang, A. Li, D.P. Wilkinson, A. Ignaszak, L. Zhang, J. Zhang, Electrochem. Energy Rev. 1 (2018) 1-34. https://doi.org/10.1007/s41918-018-0002-3

[27] N. Oturan, J. Bo, C. Trellu, M.A. Oturan, ChemElectroChem 8 (2021) 3294-3303. https://doi.org/10.1002/celc.202100588

[28] Y. Tian, M. Zhou, Y. Pan, X. Du, Q. Wang, Chem. Eng. J. 403 (2021) 126361. https://doi.org/10.1016/j.cej.2020.126361

[29] O. Scialdone, A. Galia, C. Gattuso, S. Sabatino, B. Schiavo, Electrochim. Acta 182 (2015) 775-780. https://doi.org/10.1016/j.electacta.2015.09.109

[30] Z. Ye, E. Brillas, F. Centellas, P.L. Cabot, I. Sirés, Appl. Catal. B: Environ. 257 (2019) 117907. https://doi.org/10.1016/j.apcatb.2019.117907

[31] J. Wang, C. Li, M. Rauf, H. Luo, X. Sun, Y. Jiang, Sci. Total Environ. 759 (2021) 143459. https://doi.org/10.1016/j.scitotenv.2020.143459

[32] N. Li, C. Huang, X. Wang, Y. Feng, J. An, Chem. Eng. J. 450 (2022) 138246. https://doi.org/10.1016/j.cej.2022.138246

[33] Q. Zhang, M. Zhou, G. Ren, Y. Li, Y. Li, X. Du, Nature Commun. 11 (2020) 1731. https://doi.org/10.1038/s41467-020-15597-y

[34] Y. Li, L. Liu, Q. Zhang, Y. Tang, M. Zhou, Electrochim. Acta 377 (2021) 138079. https://doi.org/10.1016/j.electacta.2021.138079

[35] H. Luo, C. Li, C. Wu, W. Zheng, X. Dong, Electrochim. Acta 186 (2015) 486-493. https://doi.org/10.1016/j.electacta.2015.10.194

[36] R.M. Félix-Navarro, M. Beltrán-Gastélum, M.I. Salazar-Gastélum, C. Silva-Carrillo, E.A. Reynoso-Soto, S. Pérez-Sicairos, S.W. Lin, F. Paraguay-Delgado, G. Alonso-Núñez, J. Nanopart. Res. 15 (2013) 1802. https://doi.org/10.1007/s11051-013-1802-3

[37] Z. Ye, D.R.V. Guelfi, G. Álvarez, F. Alcaide, E. Brillas, I. Sirés, Appl. Catal. B: Environ. 247 (2019) 191-199. https://doi.org/10.1016/j.apcatb.2019.01.029

669 [38] Y. Wang, R. Shi, L. Shang, G.I.N. Waterhouse, J. Zhao, Q. Zhang, L. Gu, T. Zhang,
670 Angew. Chem. Int. Ed. 59 (2020) 13057-13062. https://doi.org/10.1002/anie.202004841
671 [39] J. Wang, S. Li, Q. Qin, C. Peng, Proc. Natl. Acad. Sci. USA 118 (34) (2021) e2108573118.
672 https://doi.org/10.1073/pnas.210857311
673 [40] X. Zhao, X. Zhao, P. Zhu, Z. Adler, Z.-Y. Wu, Y. Liu, H. Wang, Nature Commun. 13
674 (2022) 2880. https://doi.org/10.1038/s41467-022-30337-0
675 [41] H. Dong, H. Su, Z. Chen, H. Yu, H. Yu, Electrochim. Acta 222 (2016) 1501-1509.
676 http://dx.doi.org/10.1016/j.electacta.2016.11.131
677 [42] Y. Lu, G. Liu, H. Luo, R. Zhang, Electrochim. Acta 248 (2017) 29-36.
678 http://dx.doi.org/10.1016/j.electacta.2017.07.085
679 [43] B. Garza-Campos, D. Morales-Acosta, A. Hernández-Ramírez, J.L. Guzmán-Mar, L
680 Hinojosa-Reyes, J. Manríquez, E.J. Ruiz-Ruiz, Electrochim. Acta 269 (2018) 232-240.
681 https://doi.org/10.1016/j.electacta.2018.02.139
682 [44] G.A. Kolyagin, G.V. Kornienko, V.L. Kornienko, I.V. Ponomarenko, Russ. J. Appl.
683 Chem. 90 (2017) 1143-1147. https://doi.org/10.1134/S1070427217070187
684 [45] Z. Zhang, H. Meng, Y. Wang, L. Shi, X. Wang, S. Chai, Electrochim. Acta 260 (2018)
685 112-120. https://doi.org/10.1016/j.electacta.2017.11.048
686 [46] I.M. Al-Riyami, M. Ahmed, A. Al-Busaidi, B.S. Choudri, Appl. Water Sci. 8 (2018) 199.
687 https://doi.org/10.1007/s13201-018-0846-z
688 [47] A. Xu, E. Brillas, W. Han, L. Wang, I. Sirés, Appl. Catal. B: Environ. 259 (2019) 118127.
689 https://doi.org/10.1016/j.apcatb.2019.118127
690 [48] Z. Ye, J.R. Steter, F. Centellas, P.L. Cabot, E. Brillas, I. Sirés, J. Clean. Prod. 208 (2019)
691 1393-1402. https://doi.org/10.1016/j.jclepro.2018.10.181
692 [49] Y.R. Sahu, P. Mishra, J. Chem. 2020 (2020) 4060984.
693 https://doi.org/10.1155/2020/4060984

694 [50] X. Zhou, D. Liu, Y. Zhang, J. Chen, H. Chu, Y. Qian, Chem. Eng. J. 341 (2018) 93-101.
695 https://doi.org/10.1016/j.cej.2018.01.137

Figure captions

Fig. 1. SEM images of: (a) as prepared Ni_{mesh}|C-PTFE air-diffusion electrode (ADE) and (b) same ADE after being used as cathode for three consecutive runs consisting in the electrolysis of 150 mL of 0.050 M Na_2SO_4 solutions at pH 3.0 and 25 ºC employing a cylindrical tank reactor with a Pt anode at applied current (*I*) of 100 mA. (c) EDS analysis of the pristine ADE shown in (a). (d) Change of accumulated H_2O_2 concentration in the medium with electrolysis time during each run made as described in (b). (e) Long-term assay under the same conditions described in (b) but for a single run.

Fig. 2. Normalized (a) carbenicillin (CBN) concentration and (b) TOC vs. time during the treatment of solutions of 150 mL of 0.0490 mM of the drug by: photolysis in secondary WWTP effluent (TOC_0 = 23.0 mg L^{-1}), and photoelectro-Fenton (PEF) in either 0.010 M Na_2SO_4 (TOC_0 = 10.0 mg L^{-1}), simulated water (TOC_0 = 10.0 mg L^{-1}) or secondary WWTP effluent with 0.50 mM Fe^{2+} in the three matrices. In PEF, a cylindrical tank reactor with a 3 cm^2 BDD anode and a 3 cm^2 Ni_{mesh}|C-PTFE ADE as cathode was employed at *I* = 20 mA under irradiation with a 6 W UVA lamp. All the assays were made at initial pH 3.0 and 25 ºC. (c) Accumulated H_2O_2 and active chlorine concentrations at the end of the PEF trials.

Fig. 3. Change of the normalized (a) CBN content and (b) TOC over electrolysis time for the EF and PEF treatments of 150 mL of solutions containing 0.0490 mM of the drug in simulated water with 0.50 mM Fe^{2+}, at pH 3.0 and 25 ºC, using the setup described in Fig. 2 (without lamp in EF) but at *I* = 100 mA. Time course of accumulated (c) H_2O_2 and (d) active chlorine concentrations during both trials.

Fig. 4. Effect of the anode and applied current on the variation of the normalized (a) CBN concentration and (b) TOC with electrolysis time for the AO-H_2O_2 treatment of 150 mL of solutions prepared with 0.0490 mM CBN spiked into the secondary WWTP effluent at pH 3.0

720 and 25 ºC. The assays were carried out in a cylindrical tank reactor with a 3-cm^2 Pt or BDD
721 anode and a 3-cm^2 Ni_{mesh}|C-PTFE ADE as cathode. (c) H_2O_2 and active chlorine concentrations
722 determined at the end of the above trials.

723 **Fig. 5.** Normalized (a) CBN concentration and (b) TOC removals vs. electrolysis time for the
724 EF treatment of the same drug solution described in Fig. 4 under analogous conditions, but with
725 addition of 0.50 mM Fe^{2+} as catalyst.

726 **Fig. 6.** Time course of the normalized (a) CBN concentration and (b) TOC, along with the (c)
727 accumulated H_2O_2 and active chlorine concentrations at 360 min, obtained during the PEF
728 treatment of the same drug solution described in Fig. 4 under analogous conditions, but with
729 addition of 0.50 mM Fe^{2+} as catalyst and irradiation of the solution with a 6 W UVA lamp.

730 **Fig. 7.** (a) Accumulated $^{\bullet}OH$ concentration during the AO-H_2O_2 treatment of solutions of 150
731 mL containing DMSO spiked at a concentration of 250 mM into the secondary WWTP effluent,
732 at pH 3.0, 25 ºC and *I* = 100 mA, employing a Pt or BDD anode. EF was carried out in the
733 simulated water with a BDD anode under the same conditions but with 0.50 mM Fe^{2+}. PEF was
734 analogous but with the solution illuminated with a 6 W UVA lamp. (b) Variation of Fe^{2+} and
735 Fe^{3+} concentrations during the above PEF assay in the presence of 0.049 mM CBN instead of
736 DMSO. (c) Change of the acute toxicity, measured as EC_{50}, over electrolysis time for PEF
737 treatments of 0.049 mM CBN in the secondary WWTP effluent using a BDD anode at *I* values
738 of 20 and 100 mA.

739 **Fig. 8.** Time course of the concentration of carboxylic acids detected during the (a) direct
740 photolysis, (b) EF and (c) PEF treatments of solutions of 150 mL containing 0.0490 mM CBN
741 in simulated water at pH 3.0 using a BDD anode and a Ni_{mesh}|C-PTFE ADE as cathode at *I* =
742 20 mA and 25 ºC. In EF and PEF, 0.50 mM Fe^{2+} was added as catalyst. The solution was

irradiated with a 6 W UVA lamp during the PEF assays. (d) Evolution of ammonium ion concentration under the same conditions.

Fig. 9. Reaction sequence proposed for CBN degradation in any water matrix when •OH is produced as main oxidant under EF and PEF conditions using BDD.

Fig. 10. Reaction sequence proposed for CBN degradation in water matrices containing chloride ion, giving rise to •OH and HClO as main oxidants.

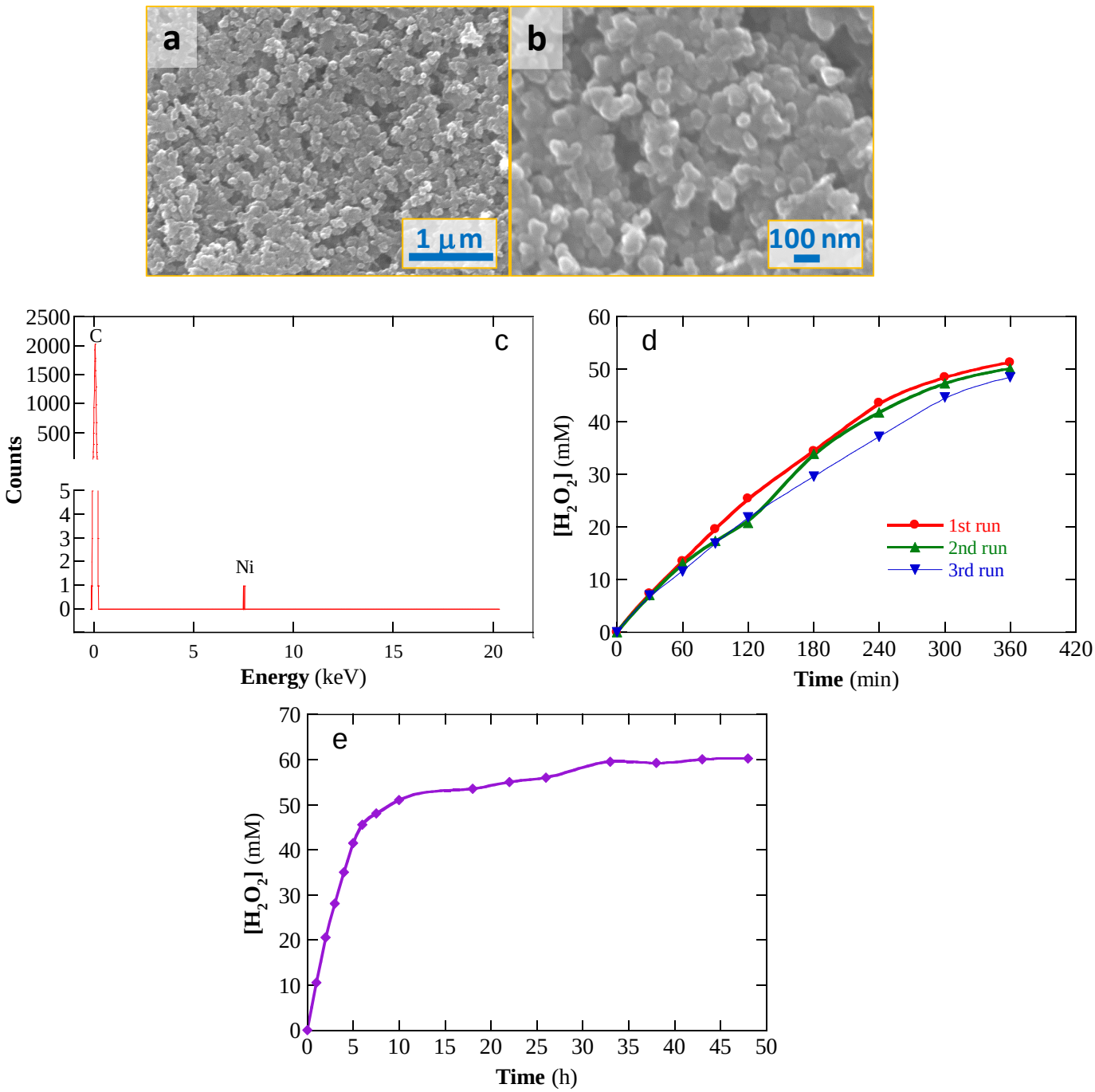
a
1 µm
b
100 nm
c
C
Ni
Counts
Energy (keV)
d
[H2O2] (mM)
Time (min)
1st run
2nd run
3rd run
e
[H2O2] (mM)
Time (h)

Fig. 1

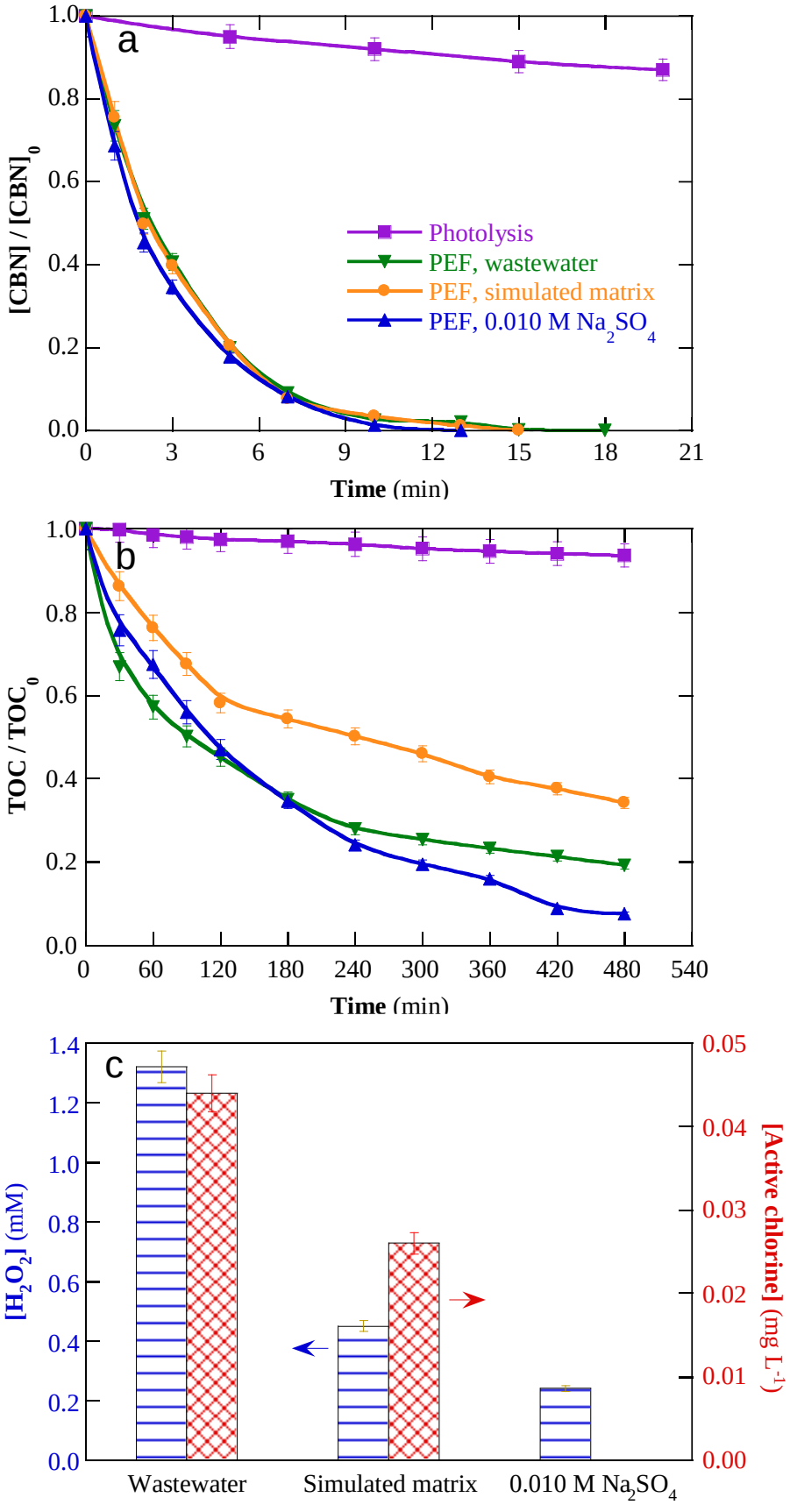
a
[CBN] / [CBN]0
Time (min)
Photolysis
PEF, wastewater
PEF, simulated matrix
PEF, 0.010 M Na2SO4
b
TOC / TOC0
Time (min)
c
[H2O2] (mM)
[Active chlorine] (mg L-1)
Wastewater
Simulated matrix
0.010 M Na2SO4

Fig. 2

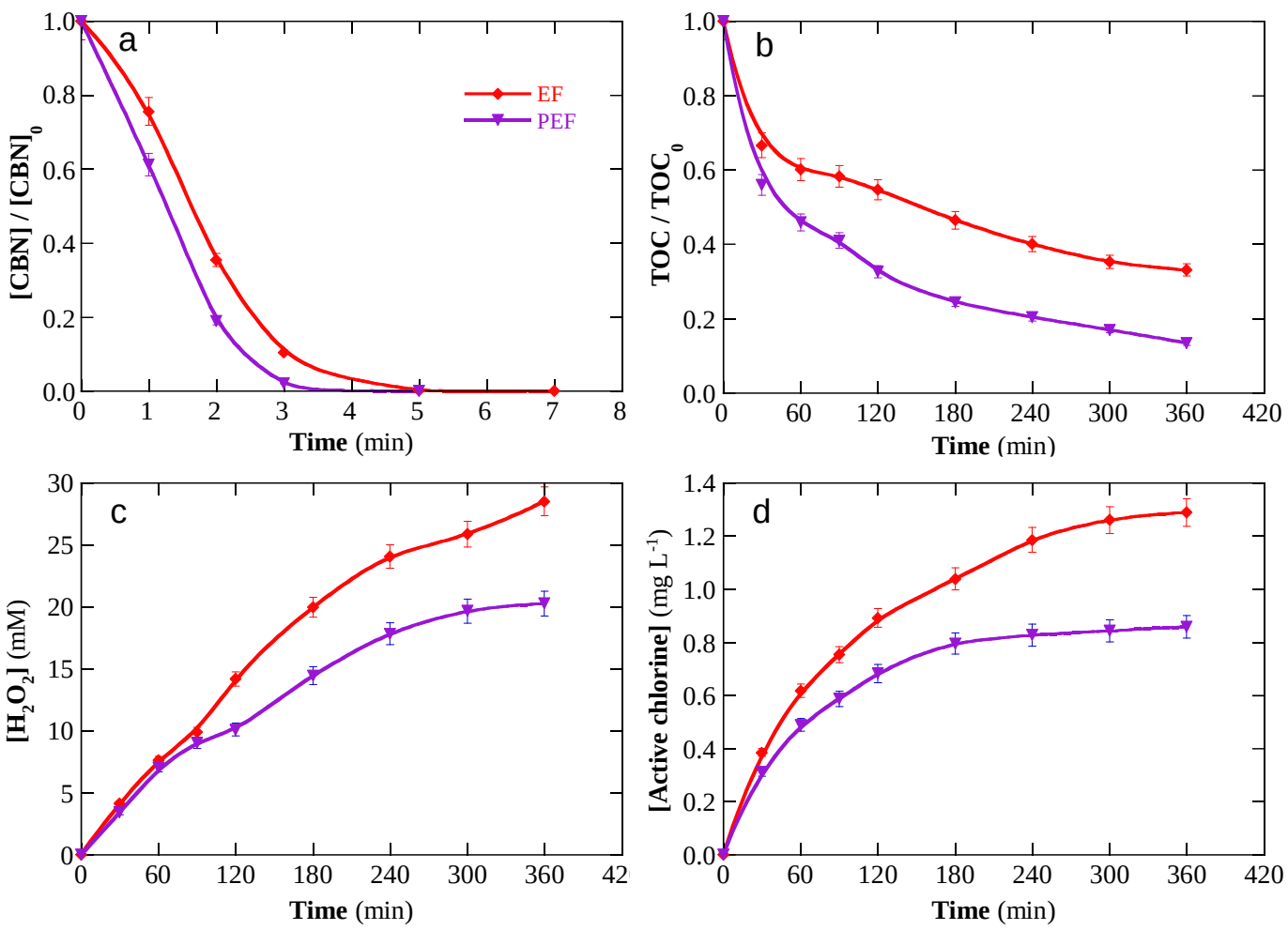
a
EF
PEF
[CBN] / [CBN]0
Time (min)
b
TOC / TOC0
Time (min)
c
[H2O2] (mM)
Time (min)
d
[Active chlorine] (mg L-1)
Time (min)

Fig. 3

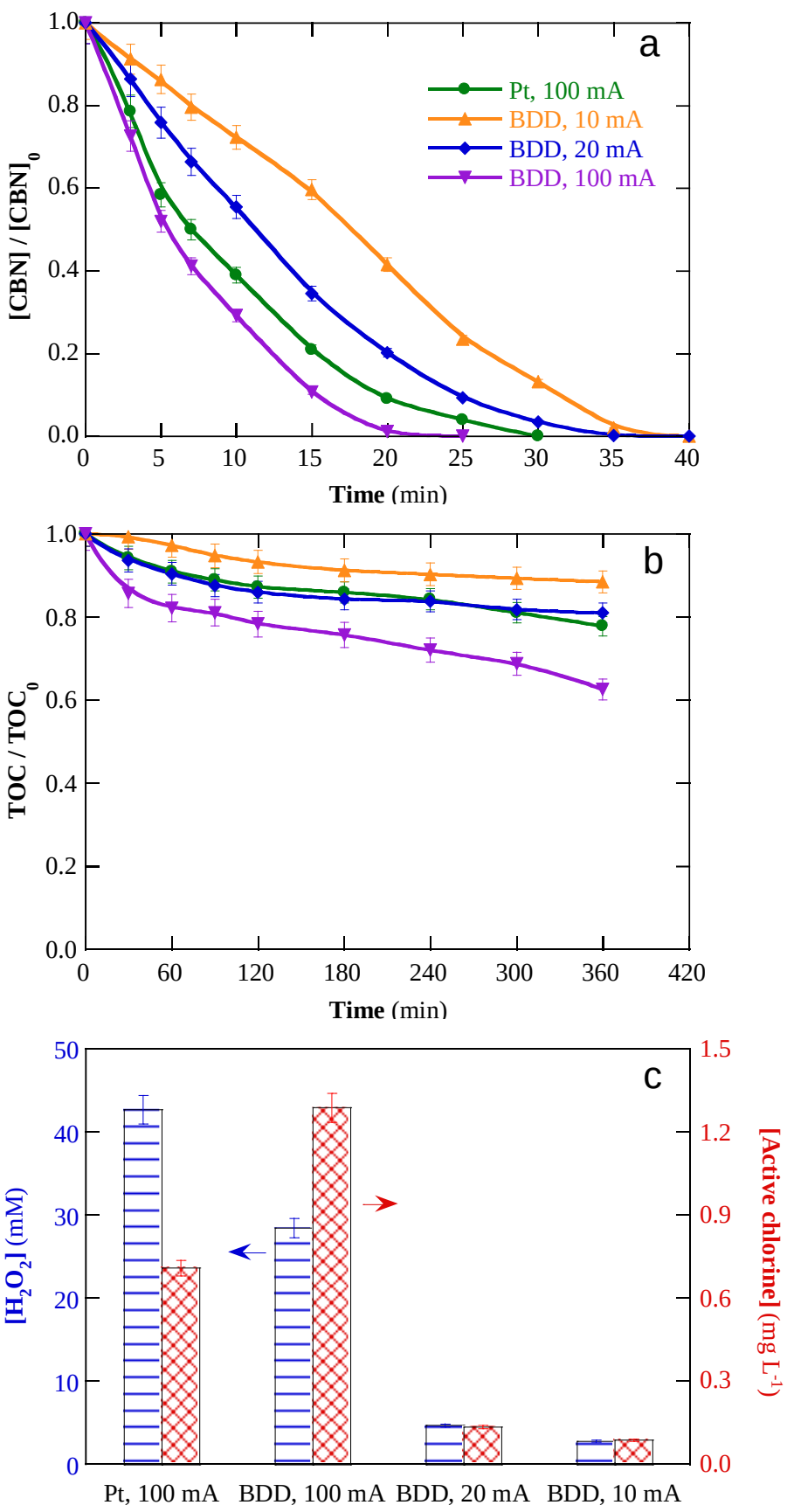
a
Pt, 100 mA
BDD, 10 mA
BDD, 20 mA
BDD, 100 mA
[CBN] / [CBN]0
Time (min)
b
TOC / TOC0
Time (min)
c
[H2O2] (mM)
[Active chlorine] (mg L-1)
Pt, 100 mA
BDD, 100 mA
BDD, 20 mA
BDD, 10 mA

Fig. 4

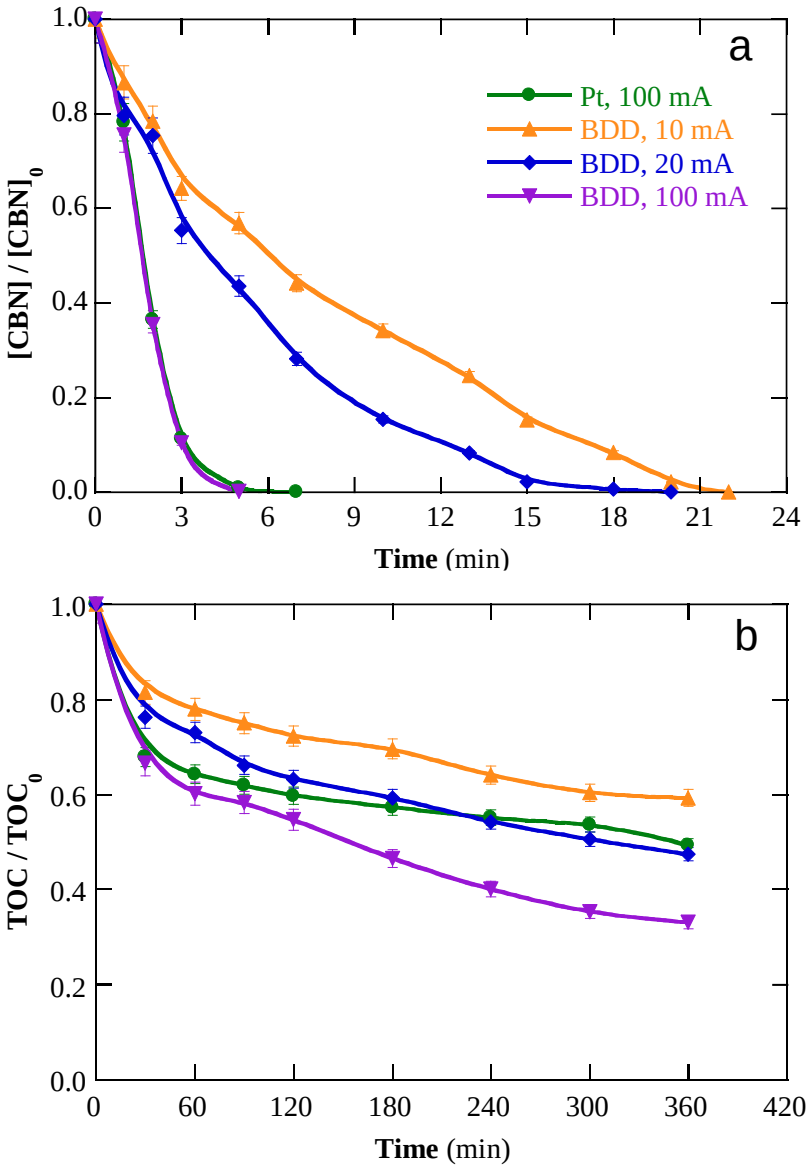
a
Pt, 100 mA
BDD, 10 mA
BDD, 20 mA
BDD, 100 mA
[CBN] / [CBN]0
Time (min)
b
TOC / TOC0
Time (min)

Fig. 5

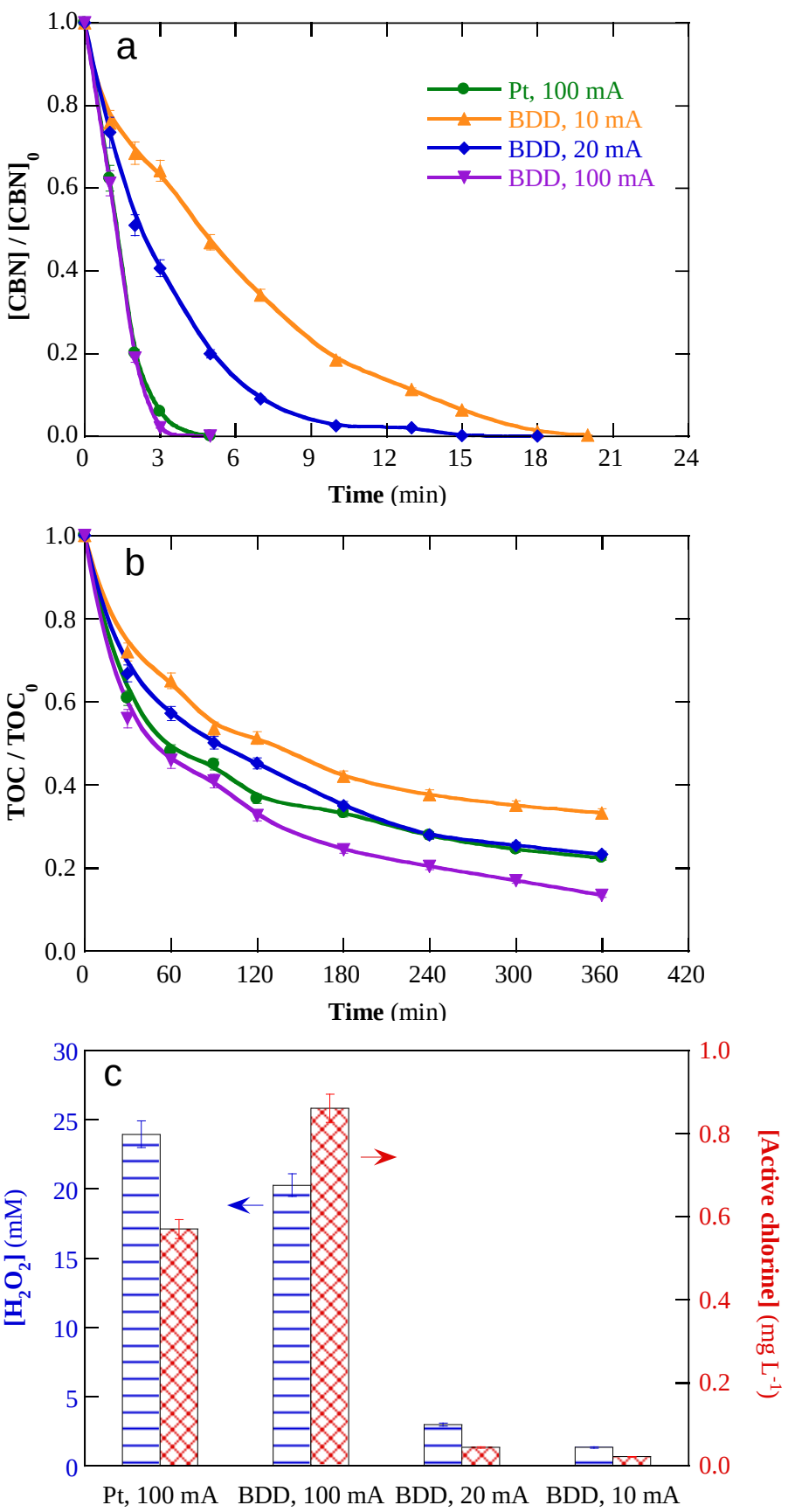
a
Pt, 100 mA
BDD, 10 mA
BDD, 20 mA
BDD, 100 mA
[CBN] / [CBN]0
Time (min)
b
TOC / TOC0
Time (min)
c
[H2O2] (mM)
[Active chlorine] (mg L-1)
Pt, 100 mA
BDD, 100 mA
BDD, 20 mA
BDD, 10 mA

Fig. 6

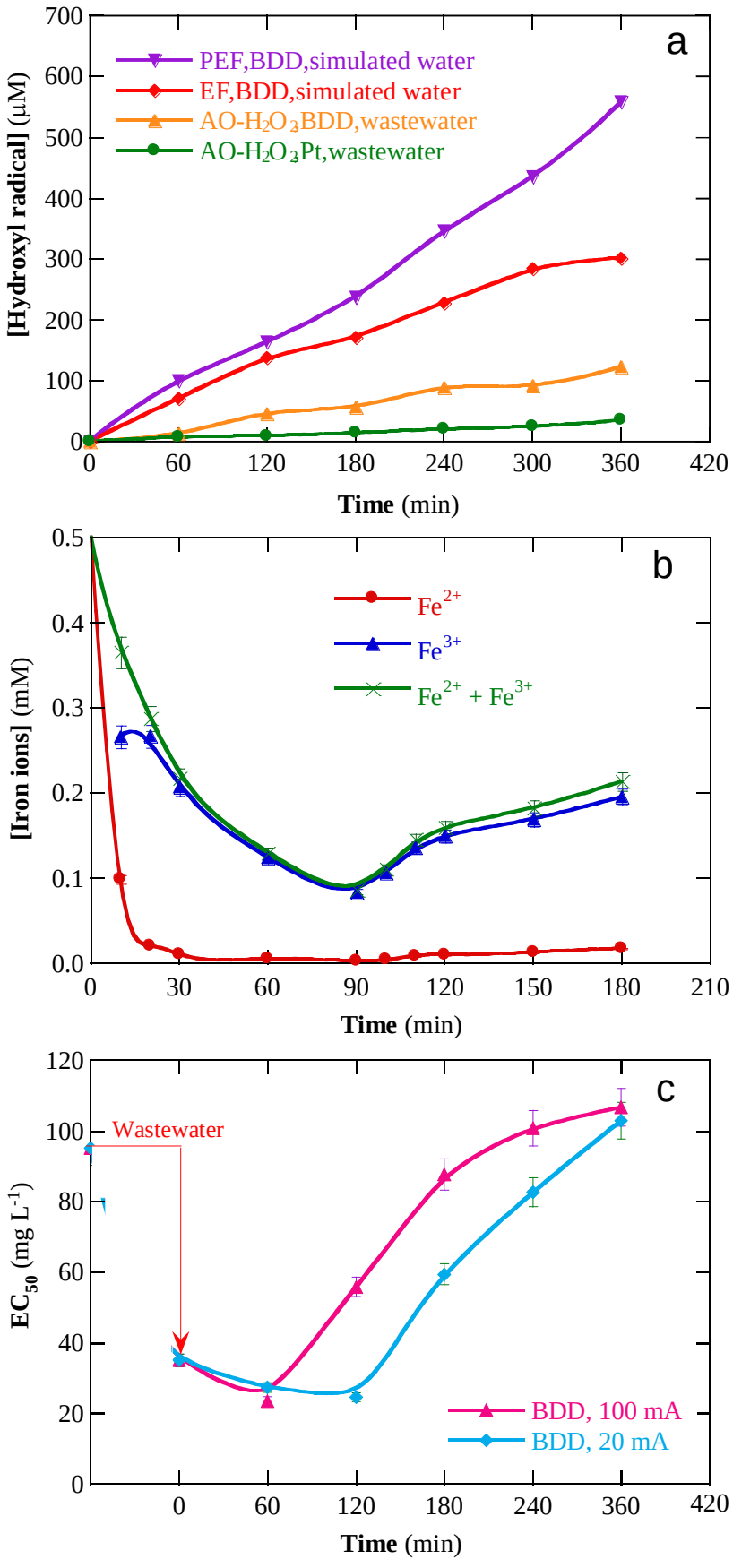
a
PEF,BDD,simulated water
EF,BDD,simulated water
AO-H2O2BDD,wastewater
AO-H2O2Pt,wastewater
[Hydroxyl radical] (μM)
Time (min)
b
Fe2+
Fe3+
Fe2+ + Fe3+
[Iron ions] (mM)
Time (min)
c
Wastewater
BDD, 100 mA
BDD, 20 mA
EC50 (mg L-1)
Time (min)

Fig. 7

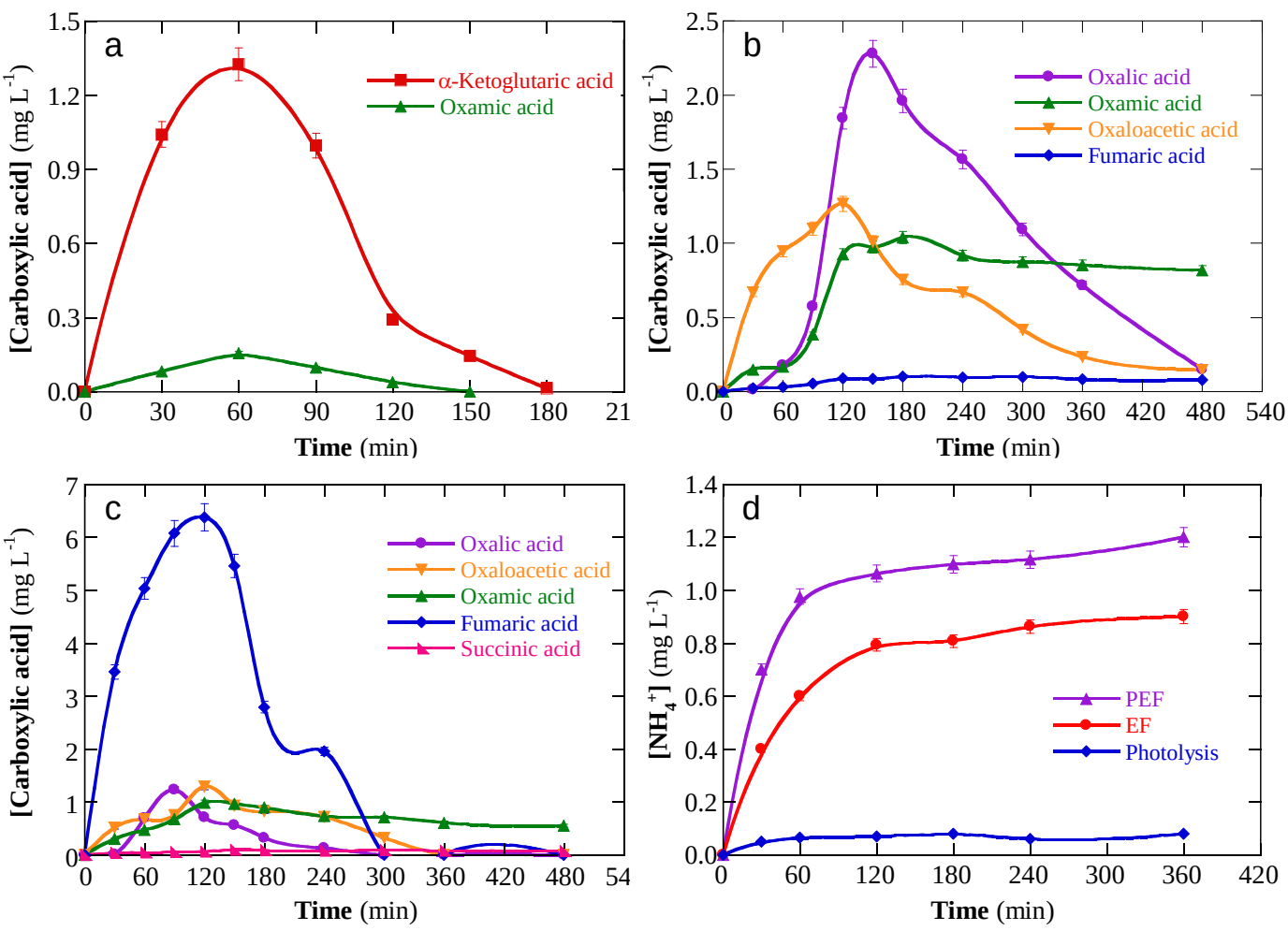
a
α-Ketoglutaric acid
Oxamic acid
[Carboxylic acid] (mg L-1)
Time (min)
b
Oxalic acid
Oxamic acid
Oxaloacetic acid
Fumaric acid
[Carboxylic acid] (mg L-1)
Time (min)
c
Oxalic acid
Oxaloacetic acid
Oxamic acid
Fumaric acid
Succinic acid
[Carboxylic acid] (mg L-1)
Time (min)
d
PEF
EF
Photolysis
[NH4+] (mg L-1)
Time (min)

Fig. 8

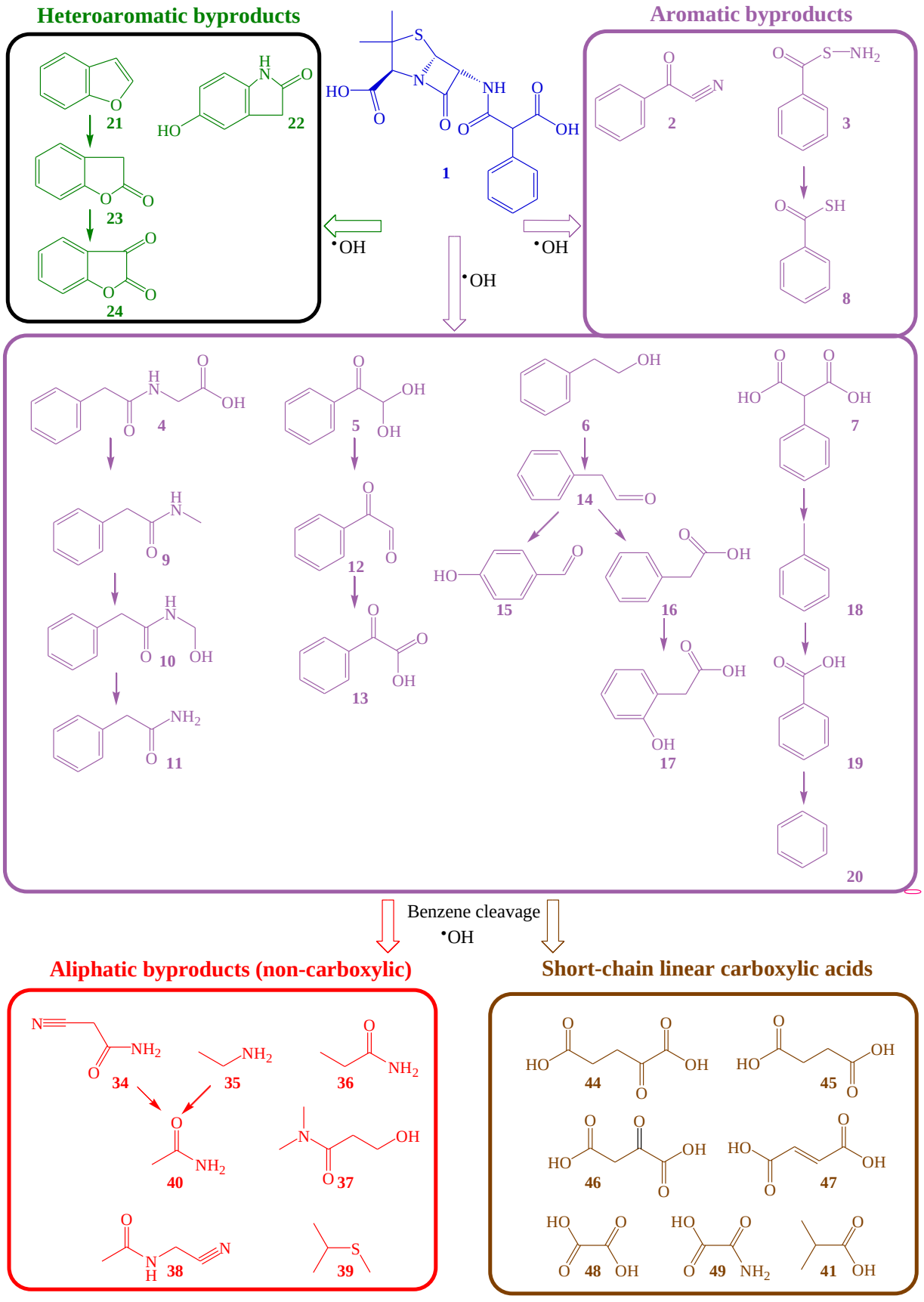
Heteroaromatic byproducts
Aromatic byproducts
•OH
•OH
•OH
Benzene cleavage
•OH
Aliphatic byproducts (non-carboxylic)
Short-chain linear carboxylic acids

938

939 **Fig. 9**

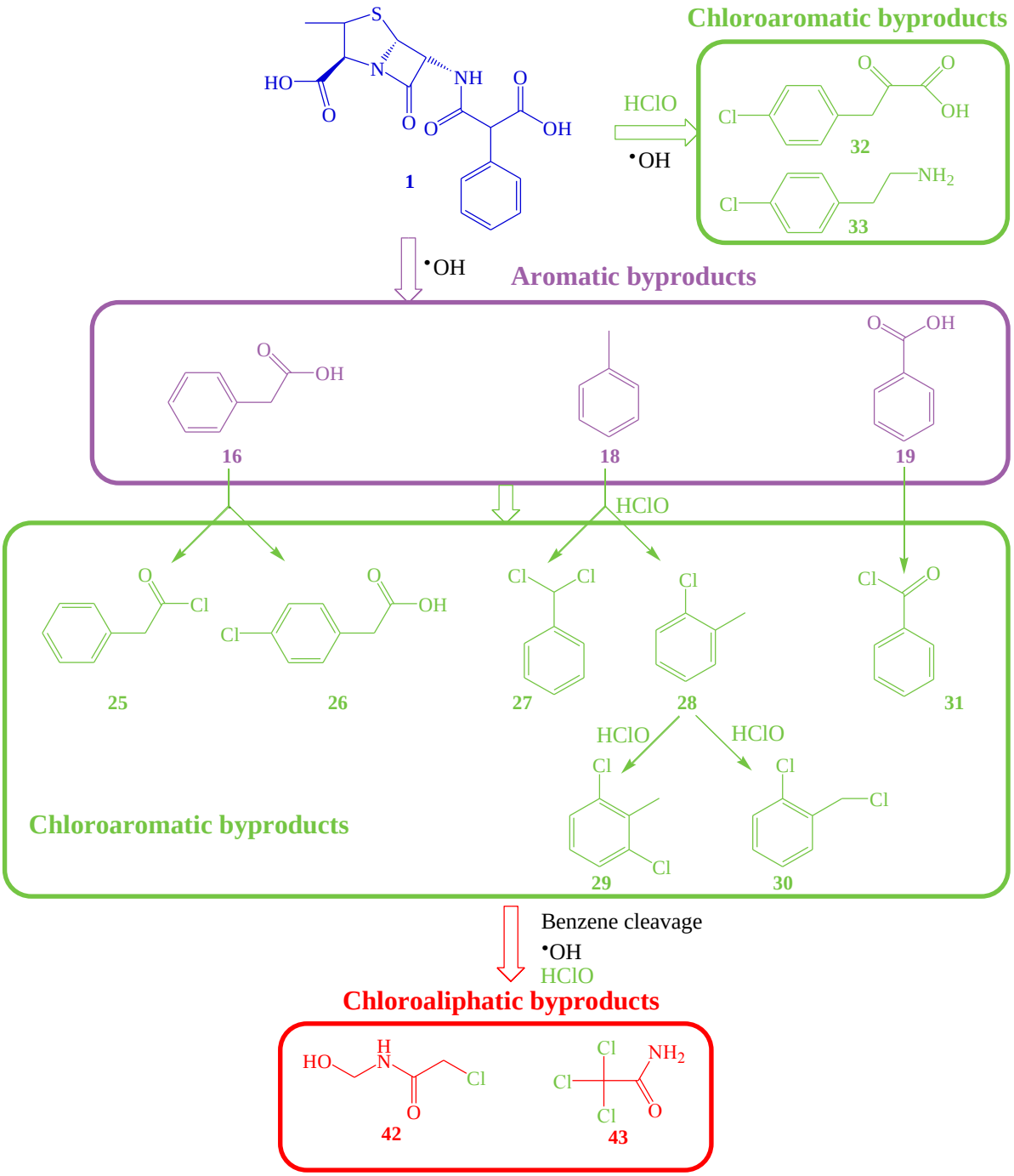

940

941

942

943

944 **Fig. 10**

945 **Table 1**

946 Pseudo-first-order rate constant for CBN decay with the corresponding *R*-squared value,
947 percentage of TOC removal, and resulting MCE and energy cost per unit TOC mass, determined
948 during the electrolysis of solutions of 150 mL containing 0.0490 mM of the drug in several
949 aqueous matrices at pH 3.0 and 25 ºC using an undivided cell equipped with a Pt or BDD anode
950 and a Ni_{mesh}|C-PTFE ADE as cathode at different applied current. The EF and PEF treatments
951 were made by adding 0.50 mM Fe^{2+}as catalyst, whereas a 6 W UVA lamp was used to irradiate
952 the solution in PEF.

Method	Anode	Current / mA	k_1 / min^{-1}	R^2	% TOC removal at 360 min	MCE (in %) at 360 min	EC_{TOC} [a] / kWh $(g\ TOC)^{-1}$
0.010 M Na_2SO_4 [b]							
PEF	BDD	20	0.180	0.985	84.0	11.4	0.634 (29.20)
Simulated water [b]							
EF	BDD	100	- [c]	- [c]	66.0	1.8	11.94
PEF	BDD	20	0.158	0.996	59.6	8.1	0.926 (41.19)
	BDD	100	- [c]	- [c]	86.5	2.3	9.11 (36.85)
Secondary WWTP effluent [d]							
AO-H_2O_2	Pt	100	0.055	0.985	22.2	-	13.5
	BDD	10	0.017	0.981	11.6	-	0.554
	BDD	20	0.035	0.984	19.0	-	1.30
	BDD	100	0.064	0.987	37.5	-	9.14
EF	Pt	100	0.413	0.992	50.8	-	5.89
	BDD	10	0.057	0.993	40.8	-	0.158
	BDD	20	0.077	0.991	52.6	-	0.469
	BDD	100	0.412	0.995	66.9	-	5.10
PEF	Pt	100	0.417	0.991	77.5	-	3.86 (17.32)
	BDD	10	0.076	0.989	66.7	-	0.097 (15.49)
	BDD	20	0.157	0.996	76.7	-	0.322 (13.93)
	BDD	100	- [c]	-	86.4	-	3.94 (16.02)

953 [a] In parenthesis, $EC_{TOC,total}$ calculated for PEF including the energy of the UVA lamp (Eq. (10));
954 [b] TOC_0 = 10.0 mg L^{-1}; [c] No linear correlation of log (c_0/c) vs. time; [d] TOC_0 = 23.0 mg L^{-1}.
955
956

957 **Table 2**

958 Results reported in the literature for the removal of organic pollutants by PEF with different

959 ADEs.

Pollutant	Electrochemical system with photoirradiation	Best results	Ref.
Acebutolol	150 mL of 0.046 mM (10 mg L^{-1} TOC) of the drug + 0.050 M Na_2SO_4 in pure water or in secondary WWTP effluent (10.4 mg L^{-1} equivalent TOC), with addition of Fe^{2+} at 0.50 mM at pH 3.0 and 25 ºC. Device: stirred tank reactor with a RuO_2 anode and a C_{cloth}|mesoporous carbon (from agarose)-PTFE at j = 10 mA cm^{-2} under 6-W UVA lamp	In pure water: total degradation in 8 min, and 87% mineralization with 7.8% MCE and EC_{TOC} = 0.485 kWh (g TOC)$^{-1}$ in 360 min. In secondary WWTP effluent: total degradation in 60 min, and 46% mineralization in 360 min	[14]
Acebutolol	150 mL of 0.046 mM (10 mg L^{-1} TOC) of the drug + 0.050 M Na_2SO_4 in pure water, with addition of Fe^{2+} at 0.50 mM at pH 3.0 and 25 ºC. Device: stirred tank reactor with a BDD anode and a C_{cloth}|N-carbon (from chitosan)-PTFE at j = 30 mA cm^{-2} under a 6-W UVA lamp	Total degradation in 20 min, and 96% mineralization with 3.5% MCE and EC_{TOC} = 4.84 kWh (g TOC)$^{-1}$ in 360 min	[24]
Carbofuran	2.5 L of 0.348 mM (50 mg L^{-1} TOC) of the pesticide + 0.050 M Na_2SO_4 in pure water or + 0.034 M Na_2SO_4 in secondary WWTP effluent (15.0 mg L^{-1} equivalent TOC), with addition of Fe^{2+} at 0.50 mM at pH 3.0 and 35 ºC. Device: pre-pilot flow plant in recirculation mode (flowrate of 200 L h^{-1}), equipped with a filter-press reactor comprising a RuO_2 anode and a C_{cloth}|carbon-PTFE cathode and a 640-mL annular glass photoreactor with a 160-W UVA lamp, at j = 50 mA cm^{-2}	In pure water: total degradation in 90 min, and 89% mineralization with 26.6% MCE and EC_{TOC} = 0.30 kWh (g TOC)$^{-1}$ in 240 min. In secondary WWTP effluent: 63% mineralization in 360 min	[20]
Bronopol	2.5 L of 0.28 mM (10 mg L^{-1} TOC) of the industrial preservative compound + 0.050 M Na_2SO_4 + 0.50 mM Fe^{2+}in pure water at pH 3.0 and 35 ºC. pre-pilot flow plant in recirculation mode (flowrate of 180 L h^{-1}), equipped with a filter-press reactor comprising a RuO_2 anode and a C_{cloth}|CoS_xP_y-MWCNT-PTFE cathode and a 640-mL annular glass photoreactor with a 160-W UVA lamp, at j = 10 mA cm^{-2}	85% degradation in 360 min, and 56% mineralization with 12.1% MCE and EC_{TOC} = 0.365 kWh (g TOC)$^{-1}$ at that time	[37]
Bisphenol-S	50 mg L^{-1} (28.8 mg L^{-1} TOC) of the chemical + 0.10 M K_2SO_4 + 0.10 mM Fe^{2+} in pure water at pH 2.5 and 25 ºC. Device: stirred tank reactor with a Pt anode and a SS_{meshh}|6% Co-carbon (from porphyrin)-PTFE at cathodic potential of -1.5 V/Ag|AgCl under UVC light (4.750 W cm^{-2})	Total degradation in 20 min, and 78% mineralization with EC_{TOC} = 6.3 kWh (g TOC)$^{-1}$ in 360 min	[17]
Carbenicillin	150 mL of 0.049 mM (10 mg L^{-1} TOC) of the drug + 0.010 M Na_2SO_4 in pure water or in secondary WWTP effluent (13.0 mg L^{-1} equivalent TOC), with addition of Fe^{2+} at 0.50 mM at pH 3.0 and 25 ºC. Device: cylindrical tank reactor with a BDD anode and a Ni_{mesh}|C-PTFE at I = 20 mA (j = 6.6 mA cm^{-2}) under a 6-W UVA lamp	In pure water: total degradation in 13 min, and 84% mineralization with 11.4% MCE and EC_{TOC} = 0.634 kWh (g TOC)$^{-1}$ in 360 min. In secondary WWTP effluent: total degradation in 18 min, and 77% mineralization in 360 min	This work

960